AD-A193 887 NONDESTRUCTIVE ANALYSIS OF MK 607 HARPOON MISSILE 1/1
CONTAINER(U) SOUTHWEST RESEARCH INST SAN ANTONIO TX
J W CARDINAL ET AL 31 AUG 87 DLA900-84-C-0910
UNCLASSIFIED F/G 13/4 NL

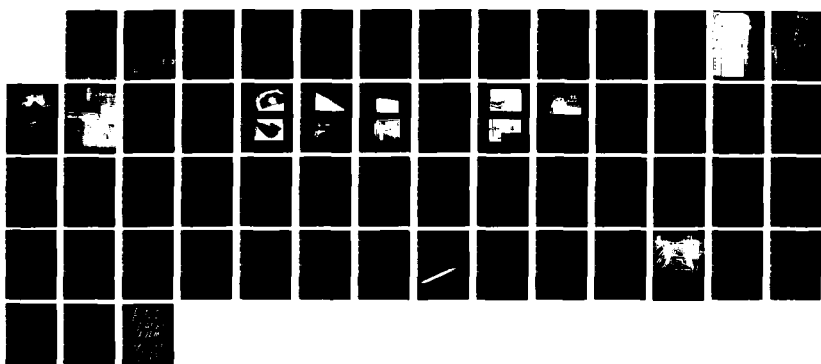

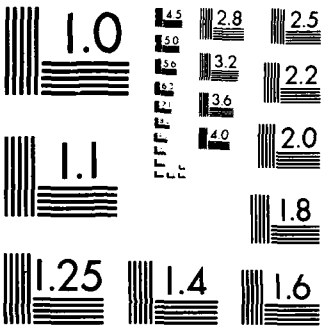
1.0
1.1
1.25
1.4
1.6
1.8
2.0
2.2
2.5
2.8
3.2
3.6
4.0
4.5
5.0
5.6

NONDESTRUCTIVE ANALYSIS OF MK 607 HARPOON MISSILE CONTAINER

By
J. W. Cardinal
S. A. Dobosz
D. J. Pomerening

FINAL REPORT
SwRI Project 17-7958-829

Prepared For
United States Navy
Pacific Missile Test Center (PMTC)
Pt. Mugu, California 93042

Performed as a Special Task for the Nondestructive Testing Information Analysis Center Under Contract No. DLA900-84-C-0910, CLIN 0001AN

August 1987

SOUTHWEST RESEARCH INSTITUTE
SAN ANTONIO HOUSTON

SOUTHWEST RESEARCH INSTITUTE
Post Office Drawer 28510, 6220 Culebra Road
San Antonio, Texas 78284

NONDESTRUCTIVE ANALYSIS OF MK 607 HARPOON MISSILE CONTAINER

By
J. W. Cardinal
S. A. Dobosz
D. J. Pomerening

FINAL REPORT
SwRI Project 17-7958-829

Prepared For
United States Navy
Pacific Missile Test Center (PMTC)
Pt. Mugu, California 93042

Performed as a Special Task for the Nondestructive Testing Information Analysis Center Under Contract No. DLA900-84-C-0910, CLIN 0001AN

August 1987

Approved:

Thomas A. Cruse, Director
Department of Engineering Mechanics

REPORT DOCUMENTATION PAGE

1a. REPORT SECURITY CLASSIFICATION Unclassified	1b. RESTRICTIVE MARKINGS
2a. SECURITY CLASSIFICATION AUTHORITY	3. DISTRIBUTION / AVAILABILITY OF REPORT Unlimited
2b. DECLASSIFICATION / DOWNGRADING SCHEDULE	
4. PERFORMING ORGANIZATION REPORT NUMBER(S) 17-7958-829	5. MONITORING ORGANIZATION REPORT NUMBER(S)
6a. NAME OF PERFORMING ORGANIZATION Southwest Research Institute 6b. OFFICE SYMBOL (*If applicable*)	7a. NAME OF MONITORING ORGANIZATION Pacific Missile Test Center
6c. ADDRESS (*City, State, and ZIP Code*) P.O. Drawer 28510 San Antonio, TX 78284	7b. ADDRESS (*City, State, and ZIP Code*) Code 1091.3 Pt. Mugu, CA 93042
8a. NAME OF FUNDING / SPONSORING ORGANIZATION Defense Logistics Agency 8b. OFFICE SYMBOL (*If applicable*) DTIC-DF	9. PROCUREMENT INSTRUMENT IDENTIFICATION NUMBER DLA900-84-C-0910; CLIN 0001AN
8c. ADDRESS (*City, State, and ZIP Code*) DTIC Cameron Station Alexandria, VA 22314	10. SOURCE OF FUNDING NUMBERS PROGRAM ELEMENT NO. / PROJECT NO. / TASK NO. / WORK UNIT ACCESSION NO.

11. TITLE (*Include Security Classification*)
Nondestructive Analysis of MK 607 HARPOON Missile Container (U)

12. PERSONAL AUTHOR(S)
J.W. Cardinal, S.A. Dobosz, D.J. Pomerening

13a. TYPE OF REPORT	13b. TIME COVERED	14. DATE OF REPORT (*Year, Month, Day*)	15. PAGE COUNT
Final	FROM June 86 TO Aug 87	August 31, 1987	54

16. SUPPLEMENTARY NOTATION
Performed as a Special Task for the Nondestructive Testing Information Analysis Center

17. COSATI CODES			18. SUBJECT TERMS (*Continue on reverse if necessary and identify by block number*)
FIELD	GROUP	SUB-GROUP	Nondestructive Evaluation, missile systems, failure analysis, structural analysis, load test, cracking

19. ABSTRACT (*Continue on reverse if necessary and identify by block number*)
Structural failures of the upper shell assembly of MK 607 HARPOON missile storage containers were investigated using analysis and experiment. The two failure modes considered were cracking in the center of the container panels and cracking and delamination near the stiffener-panel interface. Nondestructive load tests were performed on an actual container for two types of load cases: internal vacuum and externally applied concentrated loads. Finite element structural analyses were conducted to determine deflections and stresses in the container under these loading conditions. Analytically predicted deflections agreed well with experimentally measured values. The most likely cause of the panel cracking was determined to be the result of the container cover being deflected downward onto the missile support saddle bolts. This study does not identify a cause for the cracking and delamination occurring near the stiffener-panel interface. Recommendations to preclude further cracking failures in panels are provided. Areas requiring further analysis and testing are discussed.

20. DISTRIBUTION / AVAILABILITY OF ABSTRACT ☒ UNCLASSIFIED/UNLIMITED ☐ SAME AS RPT. ☐ DTIC USERS	21. ABSTRACT SECURITY CLASSIFICATION Unclassified
22a. NAME OF RESPONSIBLE INDIVIDUAL Armand J. Filer	22b. TELEPHONE (*Include Area Code*) (805) 989-8935 22c. OFFICE SYMBOL 1091.32

DD FORM 1473, 84 MAR 83 APR edition may be used until exhausted.
All other editions are obsolete.

EXECUTIVE SUMMARY

Structural failures of the upper shell assembly of MK 607 HARPOON missile storage containers were investigated using analysis and experiment. The two failure modes considered were cracking in the center of the container panels and cracking and delamination near the stiffener-panel interface. The most likely cause of the panel cracking was determined to be the result of the container cover being deflected downward onto the missile support saddle bolts. This study does not identify a cause for the cracking and delamination occurring near the stiffener-panel interface.

The implementation of operational procedures which preclude the HARPOON containers from being loaded from the exterior are recommended. In addition, potential benefits resulting from a redesign of the missile support saddle bolt configuration should be investigated. It is also recommended that the geometry and material properties of the stiffener be defined more precisely to facilitate a more accurate study of its behavior.

'Original contains color plates: All DTIC reproductions will be in black and white'

TABLE OF CONTENTS

		Page
EXECUTIVE SUMMARY		iii
LIST OF FIGURES		v
1.0	INTRODUCTION	1-1
2.0	OVERVIEW OF HARPOON CONTAINER DAMAGE	2-1
3.0	ANALYTICAL AND EXPERIMENTAL APPROACH	3-1
4.0	EXPERIMENTAL PROGRAM	4-1
	4.1 Objective	4-1
	4.2 Test Procedure	4-1
	4.3 Strain Gage Measurements	4-8
	4.4 Displacement Measurements	4-9
5.0	ANALYSIS OF THE HARPOON MISSILE CONTAINER	5-1
	5.1 Global Analysis	5-1
	5.1.1 Model Geometry	5-1
	5.1.2 Material Properties	5-1
	5.1.3 Boundary Conditions	5-3
	5.1.4 Comparison of Global Results to Experiment	5-3
	5.2 Local Analysis of Stiffener	5-12
	5.2.1 Model Geometry	5-12
	5.2.2 Material Properties	5-12
	5.2.3 Local Analysis Results	5-14
6.0	DISCUSSION OF ANALYTICAL RESULTS RELATIVE TO OBSERVED DAMAGE	6-1
7.0	RECOMMENDATIONS	7-1
8.0	REFERENCES	8-1

LIST OF FIGURES

Figure No.		Page
1-1	Schematic of HARPOON Missile Container, MK 607, Upper Shell Assembly	1-2
2-1	Photograph of Underside of Damaged Container Showing Damage to Panel and Stiffeners	2-2
2-2	Close-up Photograph of Container Exterior Showing Panel Damage (Failure Mode I)	2-3
2-3	Close-up Photograph of Container Interior Showing Panel Damage (Failure Mode I)	2-4
2-4	Close-up Photograph of Container Interior Showing Stiffener Damage (Failure Mode II)	2-5
4-1	Large Puncture in Container	4-2
4-2	Minor Damage to Side of Container	4-3
4-3	Minor Damage to End of Container	4-4
4-4	Overall View of Test Setup	4-6
4-5	Traversing Mechanism and Dial Gage on Lip	4-6
4-6	Recording Instrumentation	4-7
4-7	Container Deflections for an Equivalent Load of 1.0 psi Vacuum Using Three (3) LVDTs and a Dial Gage	4-10
4-8	Traversing Results for an Equivalent Load of 1.0 psi Vacuum Longitudinal Position is Z = 29.0 Inches	4-11
4-9	Traversing Results for an Equivalent Load of 1.0 psi Vacuum Logitudinal Position is 52.0 Inches	4-11
4-10	Traversing Results for an Equivalent Load of 1.0 psi Vacuum Longitudinal Position is 52.0 Inches (Repeat Run)	4-12
4-11	Traversing Results for an Equivalent Load of 1.0 psi Vacuum Longitudinal Position is 64.5 Inches	4-12
4-12	Traversing Results for an Equivalent Load of 1.0 psi Vacuum Longitudinal Position is 70.75 Inches	4-13
4-13	Traversing Results for an Equivalent Load of 1.0 psi Vacuum Longitudinal Position is 77.0 Inches	4-13
4-14	Traversing Results for an Equivalent Load of 1.0 psi Vacuum Longitudinal Position is 77.0 Inches (Repeat Run)	4-14

LIST OF FIGURES (Cont'd.)

		Page
4-15	Traversing Results for an Equivalent Load of 1.0 psi Vacuum Longitudinal Position is 77.0 Inches (8" Inches of Water)	4-14
4-16	Traversing Results for Concentrated Load of 200 lbs Edge Load at Z = 52.0, Displacement at Z = 56.0	4-15
4-17	Traversing Results for Concentrated Load of 200 lbs Edge Load at Z 64.5, Displacement at Z = 68.5	4-15
4-18	Traversing Results for Concentrated Load of 200 lbs Center Load at Z = 64.5, Displacement at Z = 68.5	4-16
4-19	Traversing Results for Concentrated Load of 200 lbs Center Load at Z = 77.0, Displacement at Z = 81.0	4-16
5-1	Schematic of Harpoon Container Showing Symmetry Planes and Quarter-Symmetry Finite Element Model	5-2
5-2	Longitudinal Lines for Comparison of Calculated and Measured Deflections	5-5
5-3	Comparison of Calculated and Experimentally Measured Vertical Deflections for an Internal Vacuum of 1.0 psi.	5-6
5-4	Location of 200 lb Concentrated Loads	5-7
5-5	Comparison of Calculated and Experimentally Measured Vertical Deflections for Concentrated Load Case Number 1	5-8
5-6	Comparison of Calculated and Experimentally Measured Vertical Deflections for Concentrated Load Case Number 2	5-9
5-7	Comparison of Calculated and Experimentally Measured Vertical Deflections for Concentrated Load Case Number 3	5-10
5-8	Comparison of Calculated and Experimentally Measured Vertical Deflections for Concentrated Load Case Number 4	5-11
5-9	Local Analysis Area of Container Stiffener and Corresponding Finite Element Model	5-13
5-10	Cross-sections of Container Stiffener	5-15
6-1	MK 607 HARPOON Container	6-2
6-2	Drawing of Missile Support Saddle Showing Location and Size of Protruding Bolts (from Reference [9]	6-4

1.0 INTRODUCTION

Upper shell assemblies of MK 607 HARPOON missile storage containers have recently exhibited structural failures taking the form of cracks in the fiberglass-reinforced plastic (FRP) upper shell. These failures result in the intrusion of water into the missile storage containers, thereby causing corrosion which may adversely affect the performance and reliability of the electronic components of the missile, in addition to requiring an increased level of maintenance. A schematic of the upper shell is shown in Figure 1-1, indicating the general locations of the observed cracks. Cracking and delamination has also been observed on the underside of the shell at the stiffener locations.

The objective of this program was to analyze the damage in the failed containers and suggest either design modifications and/or operational procedure changes which would preclude failures of this nature from recurring. To achieve this goal, a combined analytical and experimental approach was undertaken for the Pacific Missile Test Center (PMTC) under the auspices the Nondestructive Testing Information Analysis Center (NTIAC). In this study, full-scale, *nondestructive* tests on an actual container were performed to verify the accuracy of the structural modeling calculations.

This report gives a brief summary of the observed container damage, describes the experimental and analytical approaches used in the study, and documents the results obtained. A possible scenario which could produce the observed damage is presented. Recommendations to alleviate the problem are then presented. Areas requiring further analysis and testing are discussed.

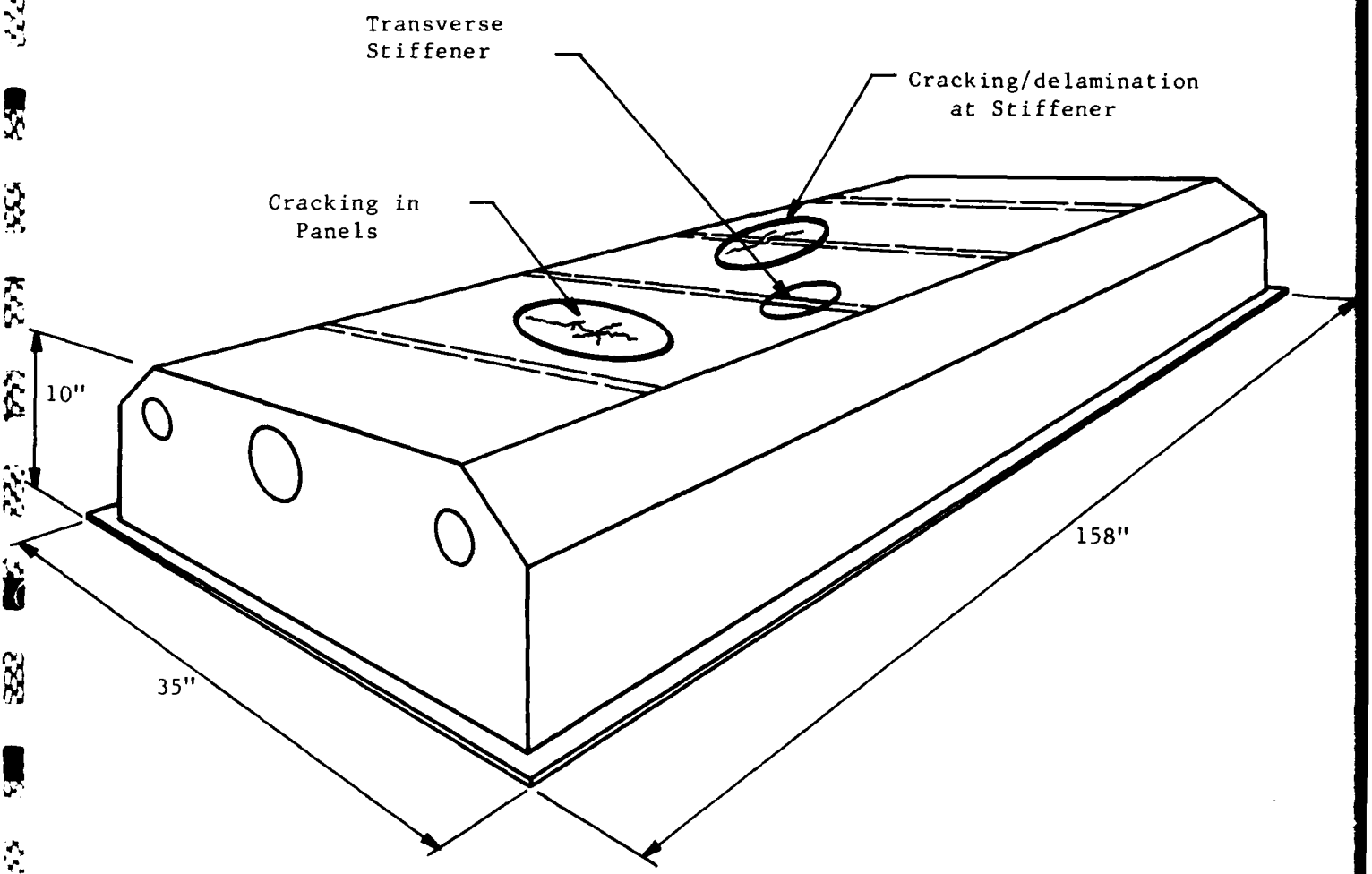

Figure 1-1 Schematic of HARPOON Missile Container, MK 607
Upper Shell Assembly

2.0 OVERVIEW OF HARPOON CONTAINER DAMAGE

Two separate modes of damage to the upper shell, or cover, of the HARPOON shipping container were investigated in this program. The first damage type (failure Mode I) considered was cracking in the middle of the container panels, away from the stiffeners. The second type (failure Mode II) involves cracking and delamination near the stiffener-panel interface. Each of these damage modes is shown in the underside view of the damaged cover given in Figure 2-1.

Figure 2-2 shows the panel cracking in failure mode I viewed from the exterior of the container, while a close-up view from the interior is shown in Figure 2-3. Note that on the container exterior, the damage appears as cracking, while the interior view seems to indicate that the damage arose from an indentation. Using the 3 X 5 index card shown in Figure 2-3 as a "scale", the two damaged areas can be measured to be about 3.5 inches apart and have an approximate diameter of 0.5 inches.

A close-up view of failure mode II is shown in Figure 2-4. The stiffener cracking, and the delamination between the stiffener and the panel, occur near mid-span as can be seen from Figure 2-1.

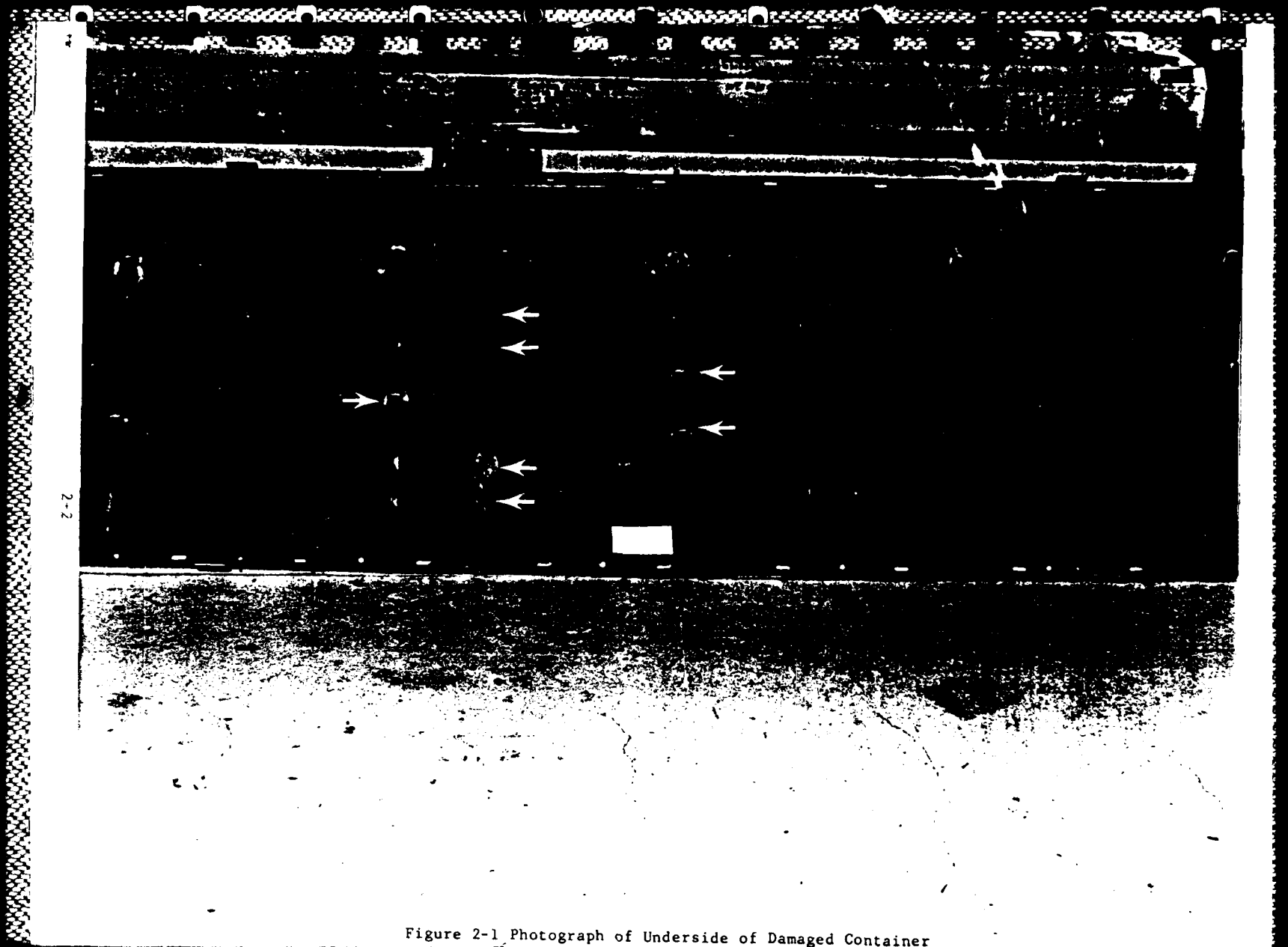

Figure 2-1 Photograph of Underside of Damaged Container

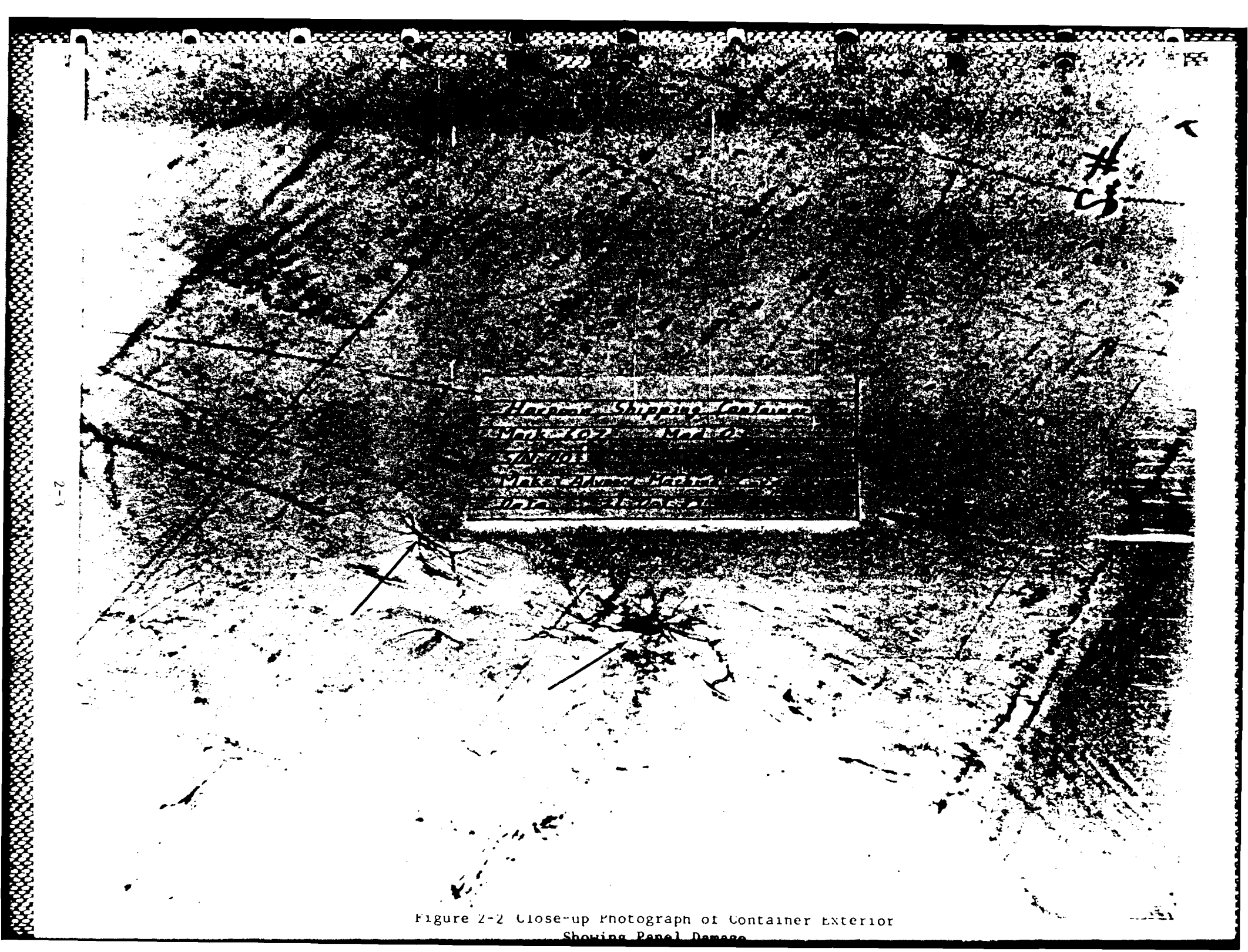

Figure 2-2 Close-up Photograph of Container Exterior Showing Panel Damage

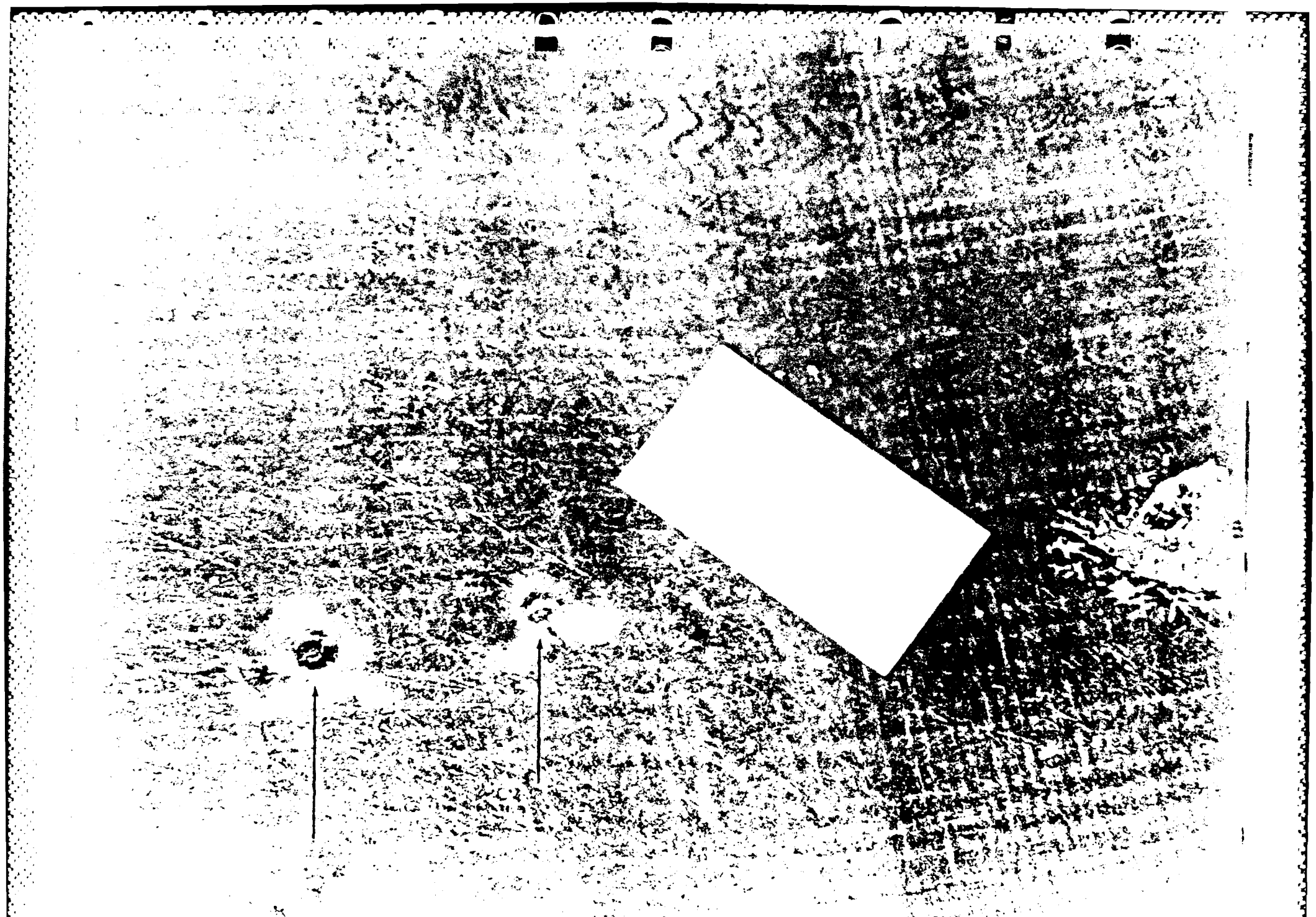

Figure 23 Close-up Photograph of Container Interior
Showing Panel Damage
(Failure Mode I)

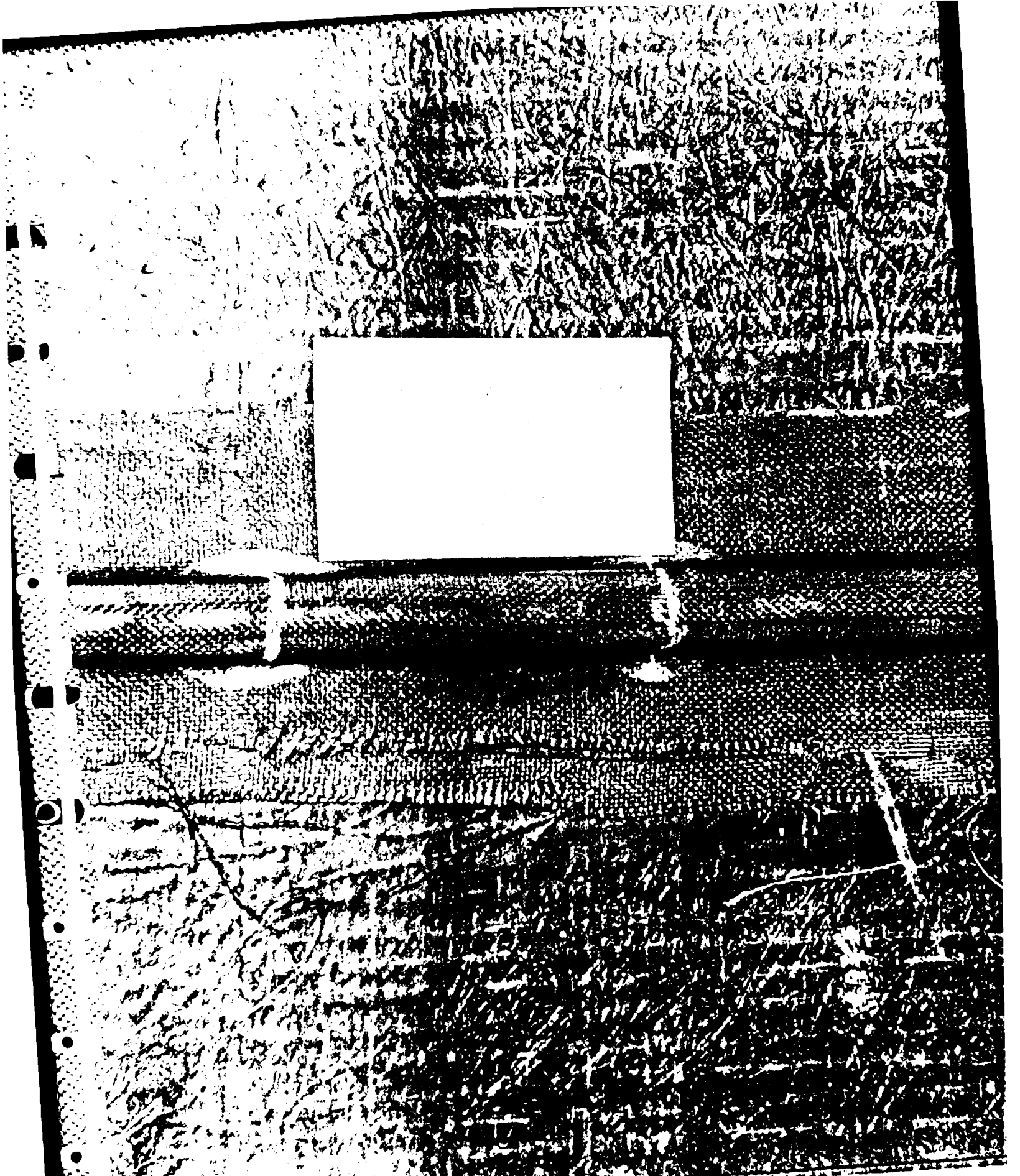

3.0 ANALYTICAL AND EXPERIMENTAL APPROACH

A combined experimental and analytical approach was selected for this investigation primarily due to uncertainties in the properties of the FRP shell material. A preliminary structural analysis of the container, subject to an internal pressure load, was performed using properties representative of typical FRP materials. This analysis gave a general indication of the deflection magnitudes that could be expected, and was an efficient way of determining the sensitivity and range needed in the displacement measurement instruments (dial gages and transducers) planned for use in the experimental program.

The objective of the experimental program was to measure the deflections in the upper shell assembly of the HARPOON container. Two loading conditions were considered: internal vacuum and externally applied concentrated load. Structural analyses were then performed for the same loading conditions to assess the predictive capability of the analysis model. Thus, it was possible to adjust the material properties and boundary conditions used in the analysis such that the model predicted the actual behavior of the container during the experiment. Having matched the experimental behavior of the container analytically, confidence was obtained in stresses and deformations calculated for the container cover.

The structural analyses of the upper shell assembly described above will be referred to in this report as "global analyses" since they considered the entire cover. More detailed analyses of the area "local" to the stiffener-panel interface were also performed.

4.0 EXPERIMENTAL PROGRAM

A HARPOON container was shipped to SwRI for use in the test program. This container was slightly damaged prior to shipment to SwRI and was available for this reason. The nature of the damage in this container was a puncture; a completely different type of damage from that being investigated in this program. Therefore, the first task was to repair this container, in accordance with standard Navy procedures [1], such that it would maintain an internal pressure or vacuum.

Primarily for reasons of safety, it was decided to apply a vacuum to the repaired container. A pressurized container would have presented a risk of an explosion. The analysis method, however, is valid for either a positive or negative internal pressure. After the container was repaired, the base and upper shell of the container were mated to provide the sealed volume for application of the vacuum. A support structure was constructed and put in place for the attachment of the displacement transducers and dial gages. Specific details regarding the test setup, displacement measurement locations, load cases and data acquisition are provided below.

4.1 Objective

The objective of the testing was to measure the deflections and strains of the upper shell assembly of the HARPOON missile container, MK 607. The deflections were to be measured under two loadings conditions: internal vacuum and a concentrated load. The results were to be used to verify material properties used in the finite element model of the upper shell.

4.2 Test Procedure

Since the missile container was received with damage to the upper shell, it was first necessary to repair the fiberglass. Views of the damage from both the exterior and interior of the shell are given in the attached photographs, Figures 4-1 to 4-3. For the large hole, it was necessary to remove the damaged fibers to obtain a good surface to bond with the new fiberglass. The region around the hole was then sanded to provide good adhesion of the new materials. Several layers of fiberglass mat were laid out with resin to cover up the hole. After this was allowed to harden, several layers of Gelcoat were applied to bring the exterior surface up to to proper

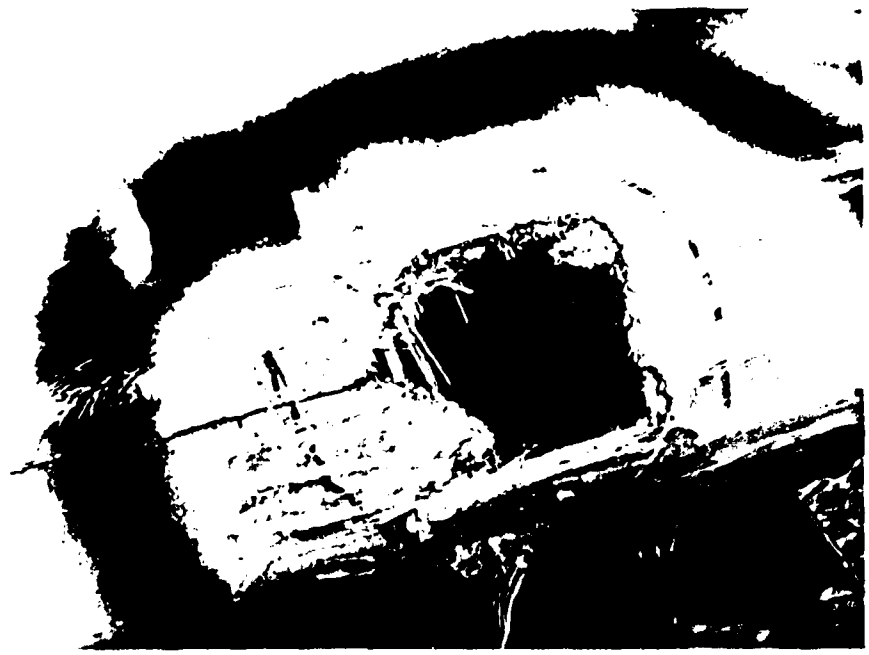

a) Exterior View

b) Interior View

Figure 4-1 Large Puncture in Container

a) Exterior View

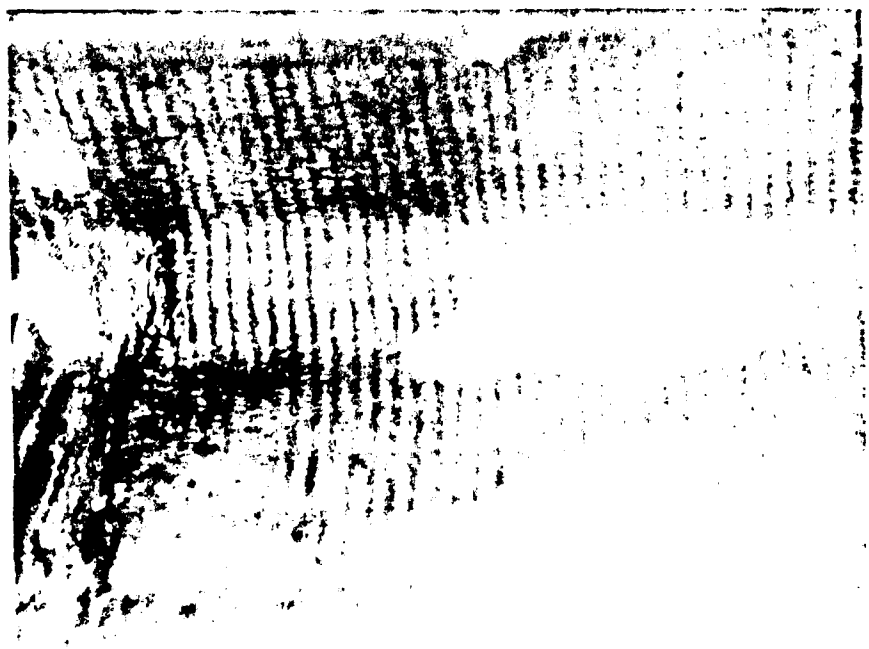

b) Interior View

Figure 4-2 Minor Damage to Side of Container

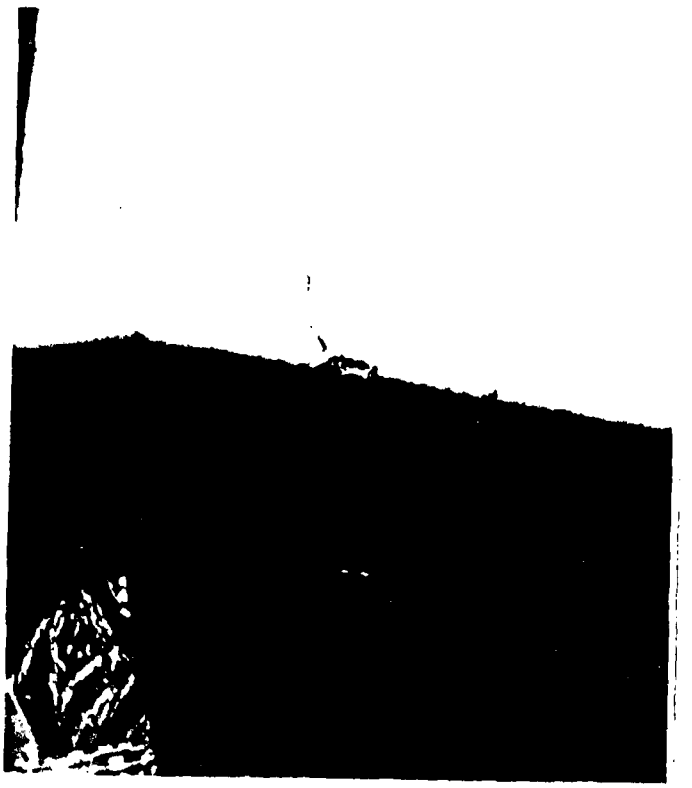

a) Exterior View

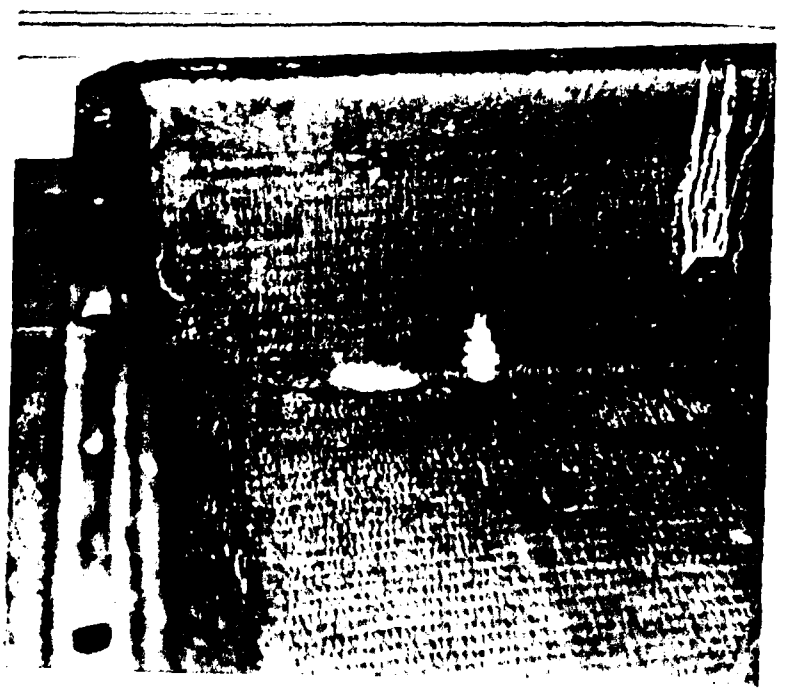

b) Interior View

Figure 4-3 Minor Damage to End of Container

level. The Gelcoat was then sanded down so that it was flush with the original structure.

There were a number of locations at which the damage was much less. For these locations, the area was sanded and several coats of Gelcoat applied to bring the surface up to the proper level. They were then sanded down to be flush with the original structure. In all cases, no painting was done to the repaired areas.

There were signs of delamination of the ribs where they intersected the sides of the container. At these locations a small amount of resin was applied to the surface to slightly reinforce the region.

Following repair of the upper shell, it was placed on the lower shell and prepared for loading. The vacuum was applied using a vacuum pump attached to a drain location on the bottom of the container. The pressure differential, ambient versus internal, was read using a water manometer attached to a port placed in the humidity indicator and pressure relief hole in one end of the shell. The amount of vacuum was controlled by adjusting a valve in the vacuum line so that the required pressure was obtained.

Strain gages were placed at two locations on the top surface of the shell. One was placed on the center rib at the transverse centerline of the shell. The second was placed at station 107", which is 1/4 of the way between two ribs on the transverse centerline of the shell. The strains were measured using a Vishay bridge completion and display unit. The gages used were 1/4" gages with 120 ohms of resistance made by Micro-Measurements.

Displacements were measured using a dial gage on the lip of the upper shell and linear variable differential transformer (LVDT) displacement transducers on the top of the shell. The dial gage was attached to a support structure (Figures 4-4 and 4-5) and read directly. The Schaevitz LVDT's were powered using a DC power supply and the output monitored on digital voltmeters. The output of one on the LVDT's could also be fed into a X-Y plotter for display as a function of transverse distance on the container top. Some of the equipment is shown in Figure 4-6.

Two series of tests were performed. In the first, three LVDT's were attached to a support structure which was suspended above the top of the upper shell. These were located at the centerline, quarter point and edge of the shell, with the edge defined as the location where the upper shell began to angle down. Prior to testing, the outputs of each of the transducers were

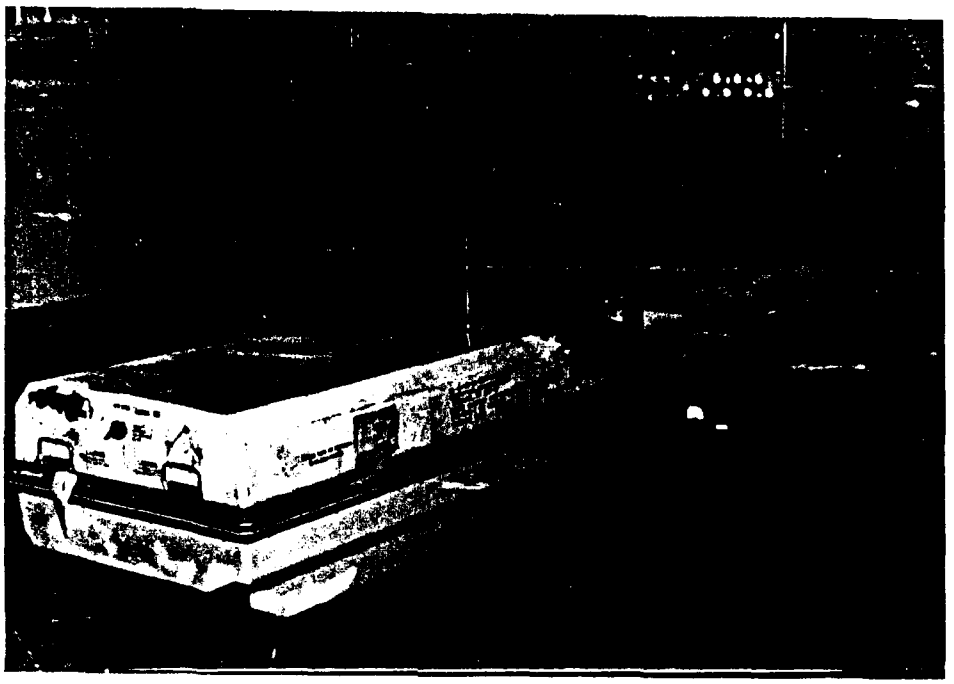

Figure 4-4 Overall View of Test Setup

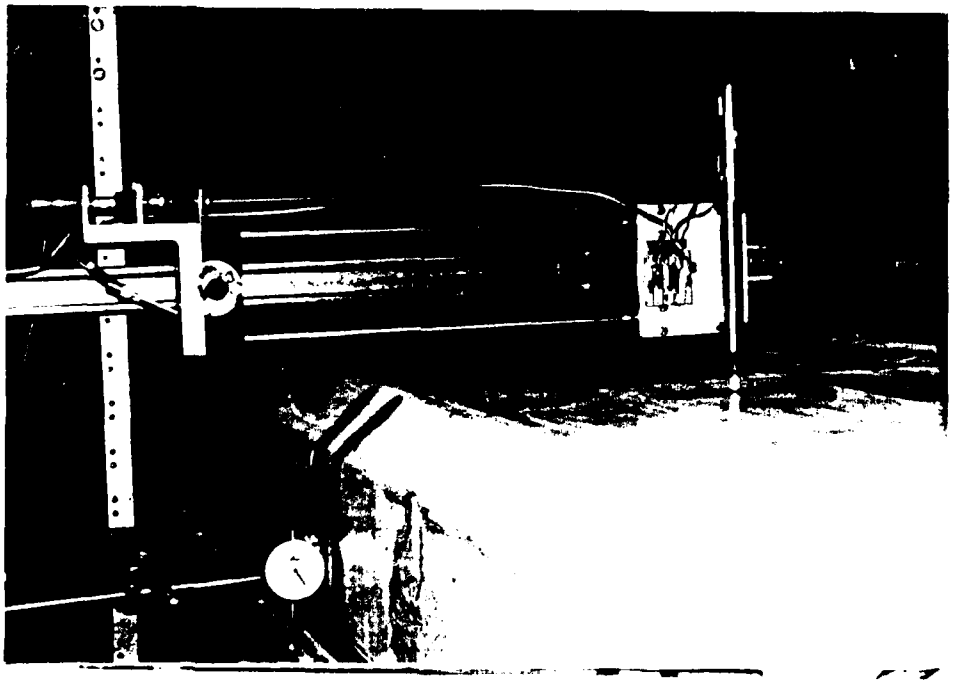

Figure 4-5 Traversing Mechanism and Dial Gage on Lip

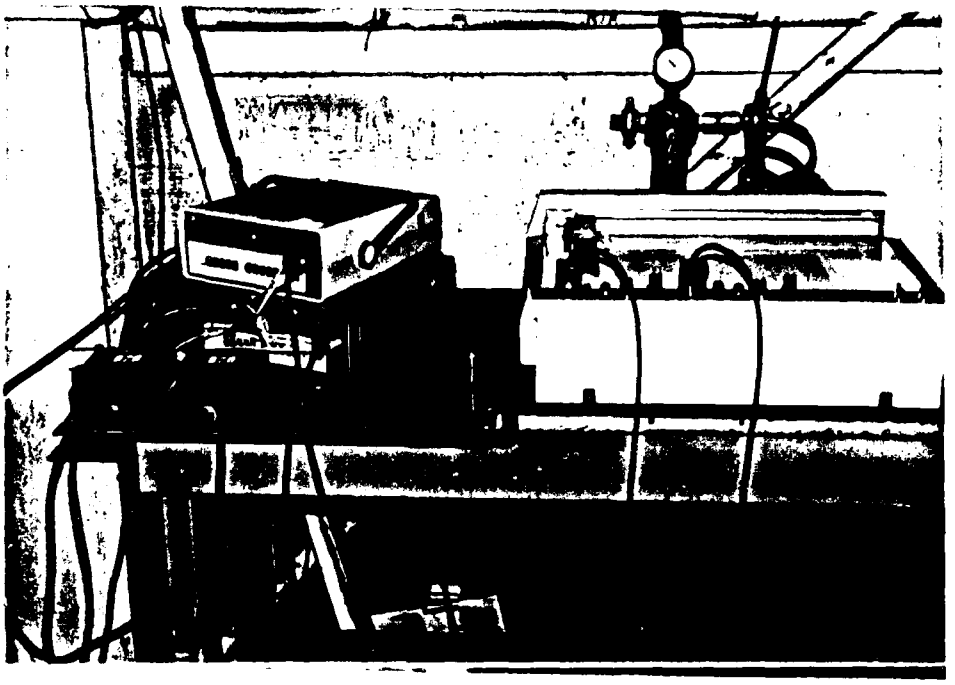

Figure 4-6 Recording Instrumentation

zeroed and the load applied. After the load was applied and the deflection allowed to stabilize, the output of each of the transducers was recorded. The load was then released and the support structure moved along the length of the container so that measurements could be made at various longitudinal positions.

A number of questions arose as a result of the first series of tests. In an attempt to answer some of these, a second setup was developed in which one LVDT was traversed across the top of the shell from the centerline to the edge at one give longitudinal position. The test setup is shown in the photographs. For this series of tests, the output of the LVDT was recorded on the X-Y plotter as a function of the transverse distance along the top. Two plots were made for each longitudinal position corresponding to zero and 14 inches of water (0.5 psi) differential pressure.

Using the traversing displacement measuring system, a second loading condition was applied. This concentrated load consisted of ten 20-lb weights placed at defined locations on the upper shell. The weights contacted the surface of the shell on a rectangular area with semicircular ends. The rectangle was 7-3/4" long and 2-7/8" wide. The displacements as a result of this concentrated load were measured four inches to one side of the centerline of the load.

4.3 Strain Gage Measurements

As noted previously, the strain gages were mounted on the top surface of the shell at the transverse centerline. Strain measurements were taken only for the internal vacuum loading condition. For the gage located* over the center rib, Z = 77.0, the strains measured were: longitudinal = 3650 in/in/psi and lateral = -2640 in/in/psi, where a positive strain represents tension. These strains have been scaled to an equivalent 1.0 psi loading. It is interesting to note that lateral strain is compressive, which indicates that the rib has a significant influence on the local strain response. The tension-compression couple in the rib under the internal vacuum will have a compressive component on the top surface. Between the ribs, Z = 107.0, both the strains are tension: longitudinal = 870 in/in/psi and lateral = 690

*In the experiments, measurement locations were defined relative to the end of the shell with the desiccant container.

in/in/psi.

4.4 Displacement Measurements

From the preliminary set of displacement measurements obtained using the three LVDT's and the dial gage shown in Figure 4-7, a number of conclusions were drawn. Note that the measurements were made for 14 inches of water (approximately 0.5 psi). The data given has been scaled to correspond to a loading of 1.0 psi; i.e., the original data has been multiplied by a factor of two. Some deflection is measured at the lip, the metal rim where the upper shell attaches to the lower shell. This deflection is small, less than 0.1 inches.

As expected, the amount of deflection increases closer to the transverse centerline of the shell. It can also be seen that the rib locations at 29, 53, 77, 102 and 126 have less deflection than that measured between the ribs. In addition, the amount of deflection generally increases as one goes from the end of the shell to the longitudinal centerline, with little deflection measured at the end. One point observed was that there was significant deflection at the edge of the top shell. To improve the measurement of the displacement pattern, it was necessary to go to the traversing mechanism.

It was also noted that there was significant difference in the measured deflection about the longitudinal centerline of the shell. What can be considered pairs of ribs at 29 and 126, as well as 53 and 102, showed differences in measured deflections for the same loading condition. Some differences can be attributed to the presence of the desiccant container at one end, but it is not expected that this would account for all the differences. It was concluded that the most probable cause of the differences was variations in the construction of the shell. The composite fiberglass rib and shell structure is difficult to manufacture uniformly and it is estimated that there may be variations of 30% in the stiffness. The major differences will be associated with the construction of the ribs and their attachment to the shell.

Results of the traversing mechanism measurement for various longitudinal locations are given in Figures 4-8 to 4-19. Displacements are presented for both the vacuum and concentrated loading conditions. The first thing to notice is the fact that the zero load deflection is different than expected. From the drawings of the shell supplied, there should be a crown at

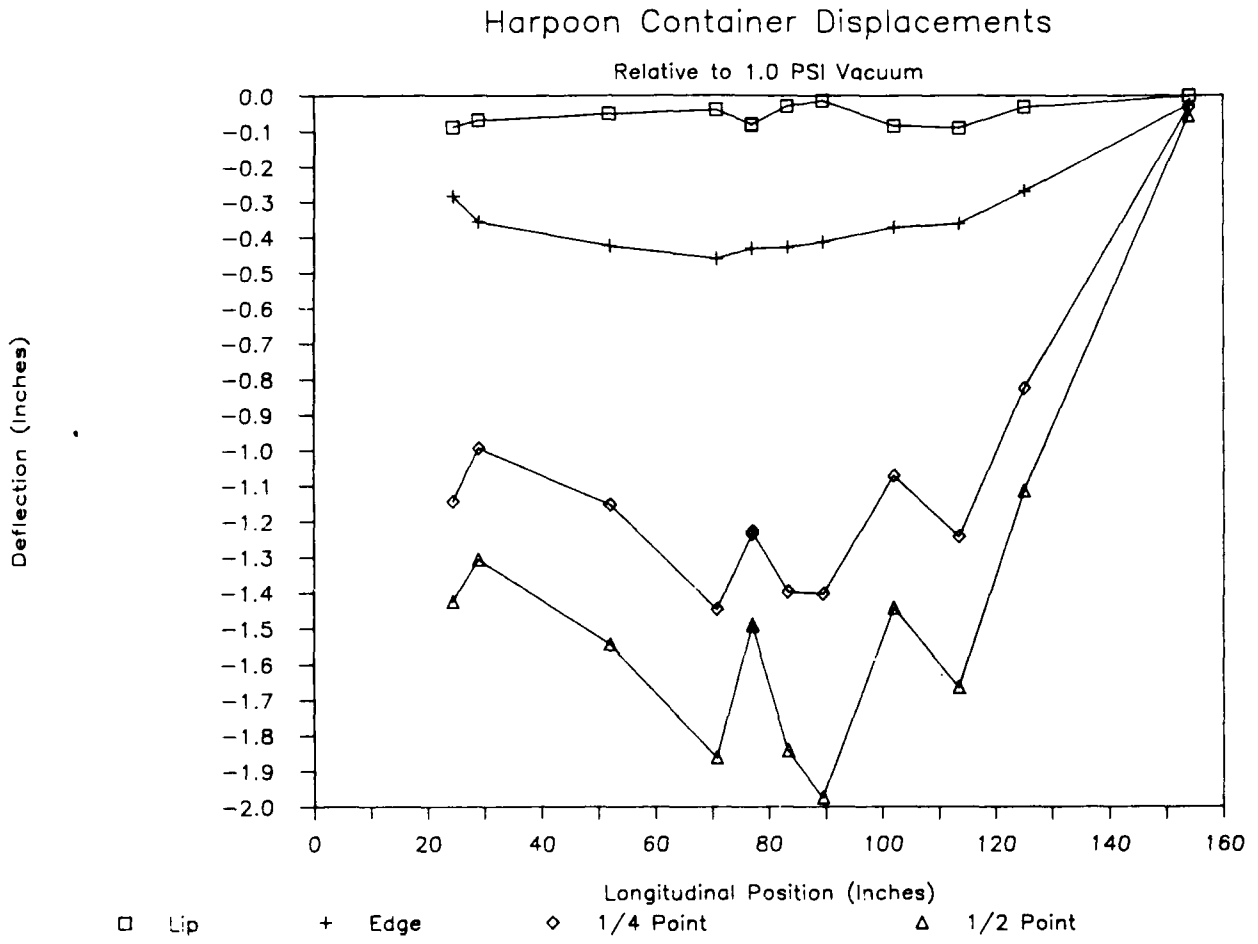

Figure 4-7 Container Deflections for an Equivalent Load of 1.0 psi Vacuum Using Three (3) LVDTs and a Dial Gage

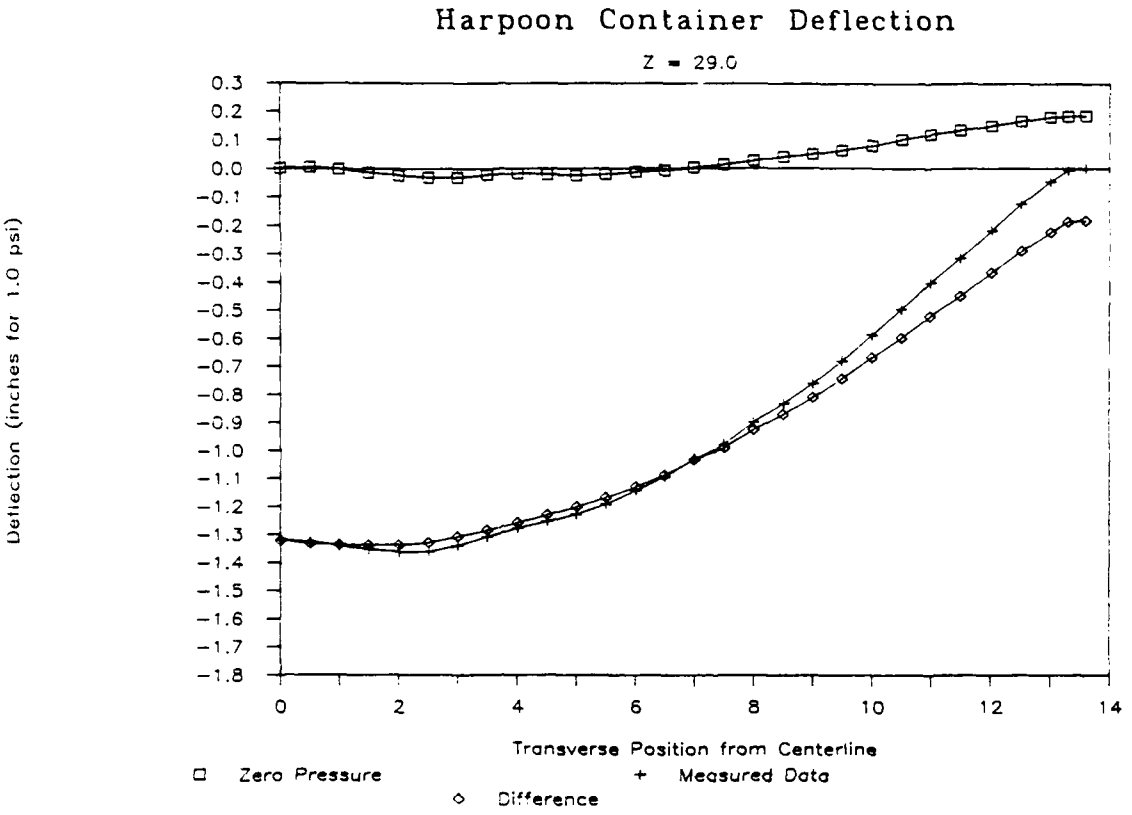

Figure 4-8 Traversing Results for an Equivalent Load of 1.0 psi Vacuum Longitudinal Position is Z = 29.0 Inches

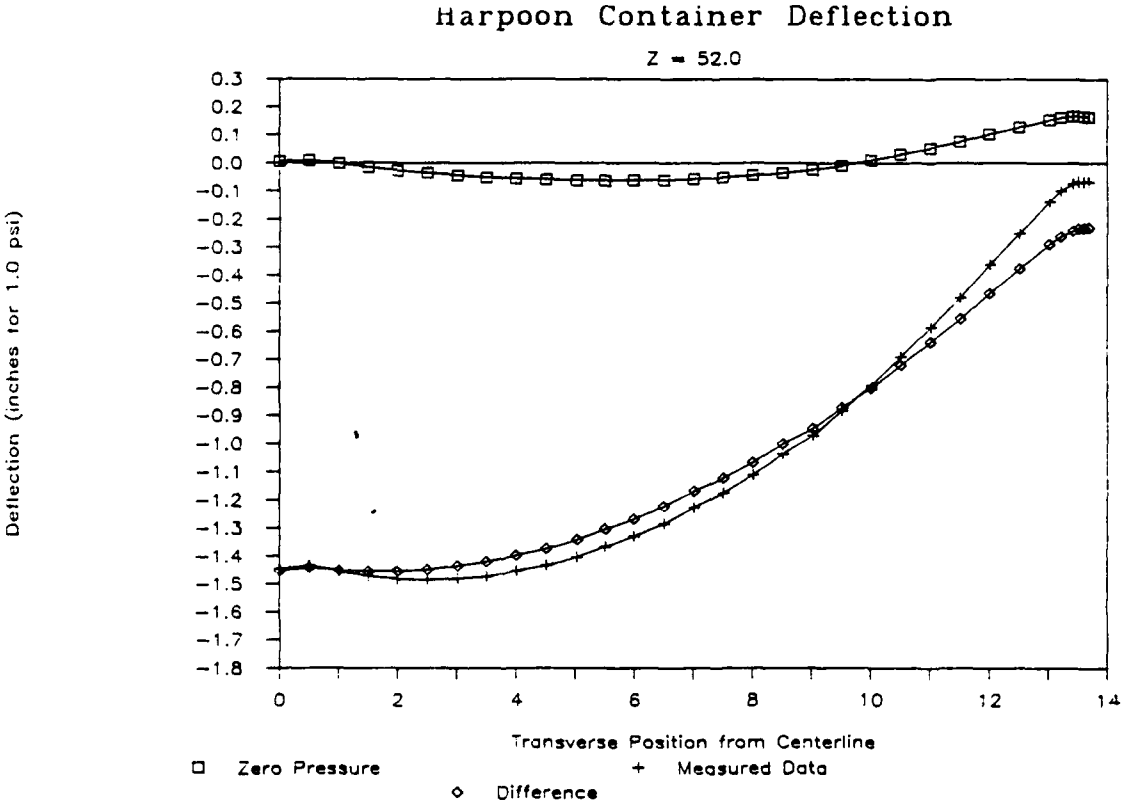

Figure 4-9 Traversing Results for an Equivalent Load of 1.0 psi Vacuum Longitudinal Position is 52.0 Inches

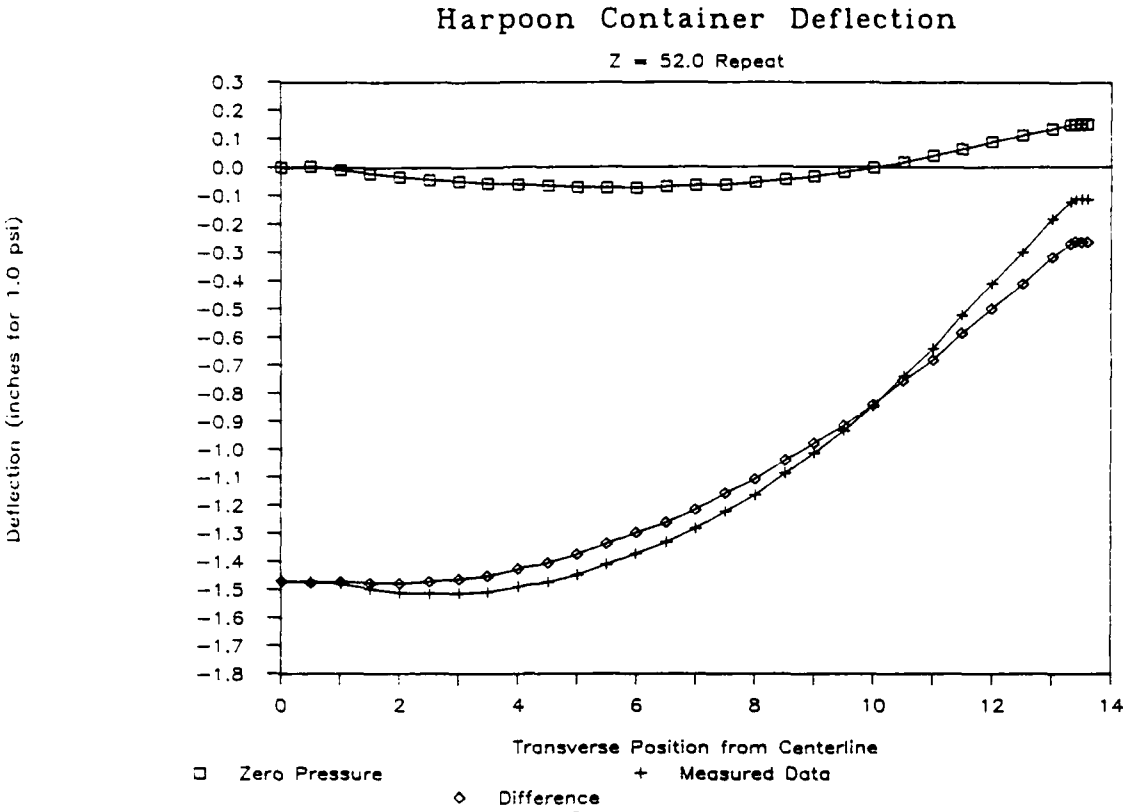

Figure 4-10 Traversing Results for an Equivalent Load of 1.0 psi Vacuum Longitudinal Position is 52.0 Inches (Repeat Run)

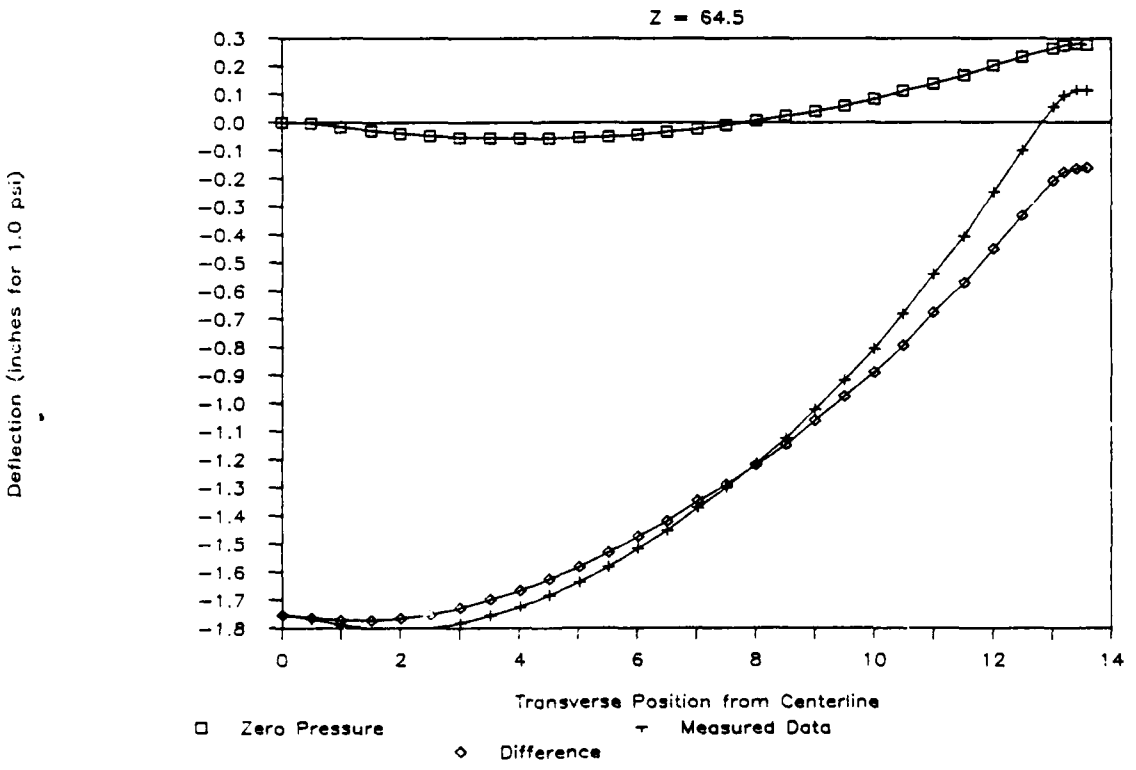

Figure 4-11 Traversing Results for an Equivalent Load of 1.0 psi Vacuum Longitudinal Position is 64.5 Inches

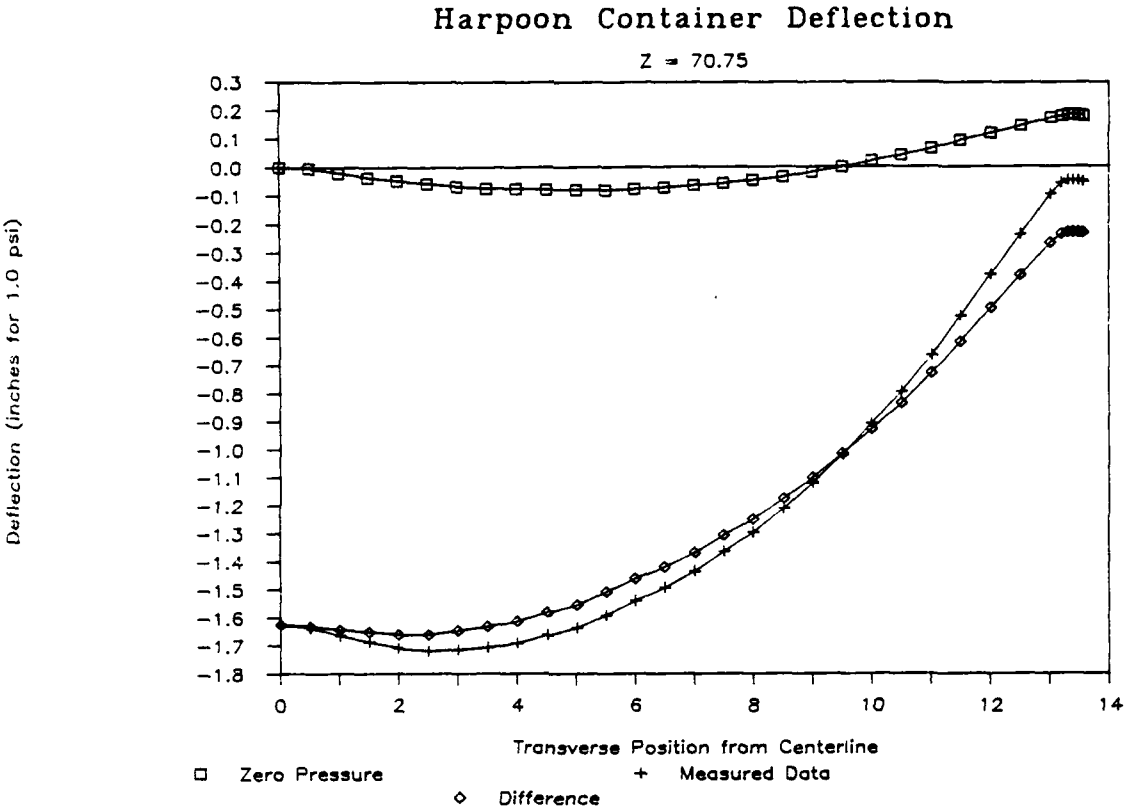

Figure 4-12 Traversing Results for an Equivalent Load of 1.0 psi Vacuum Longitudinal Position is 70.75 Inches

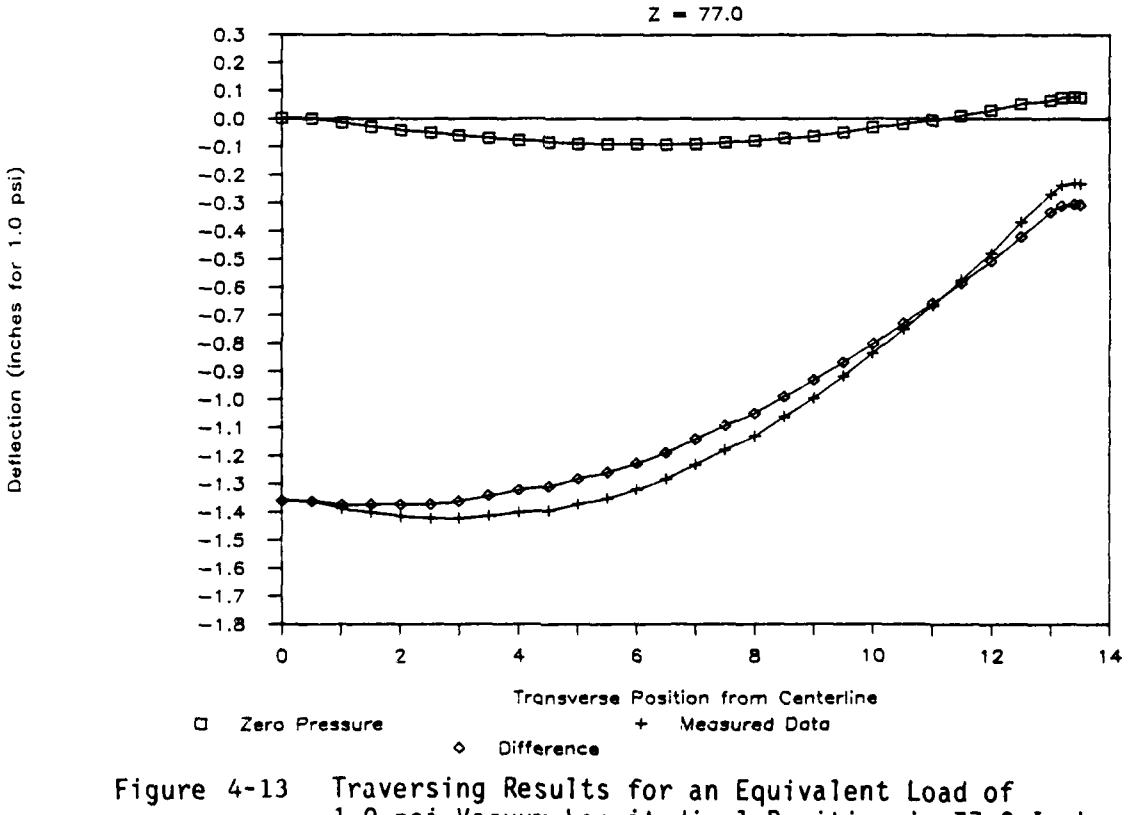

Figure 4-13 Traversing Results for an Equivalent Load of 1.0 psi Vacuum Longitudinal Position is 77.0 Inches

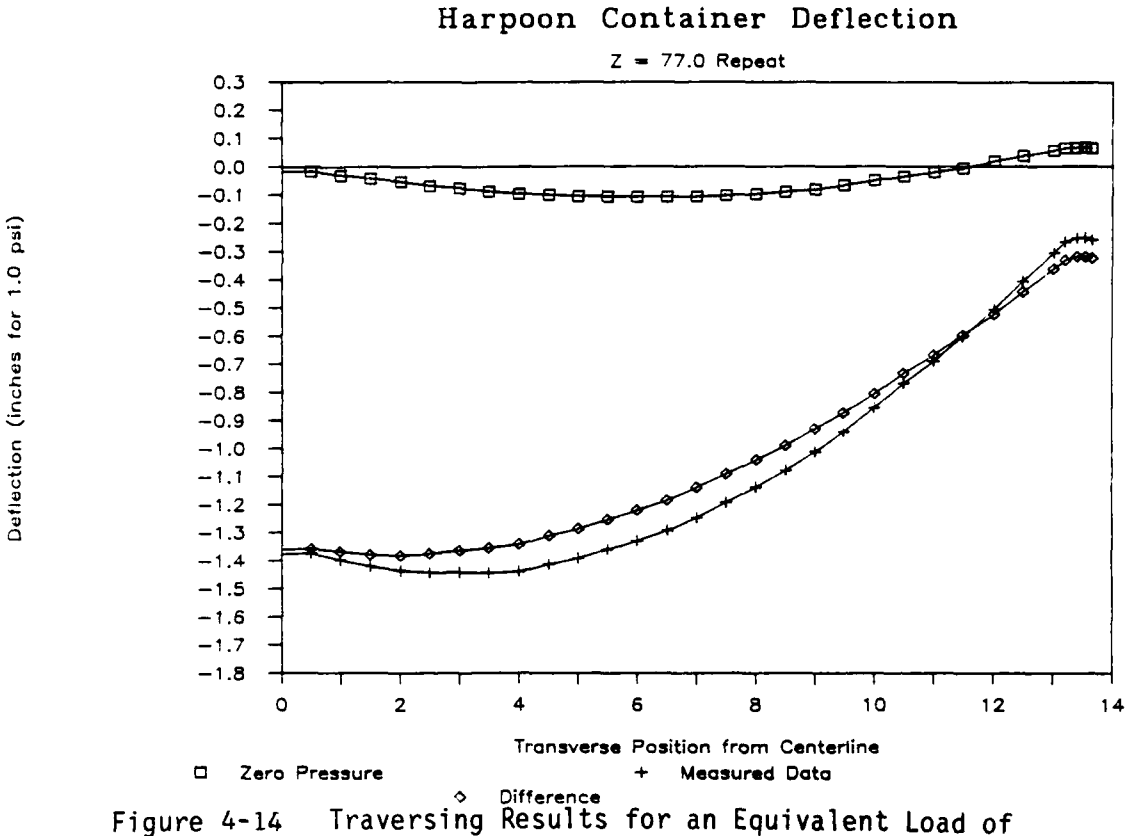

Figure 4-14 Traversing Results for an Equivalent Load of 1.0 psi Vacuum Longitudinal Position is 77.0 Inches (Repeat Run)

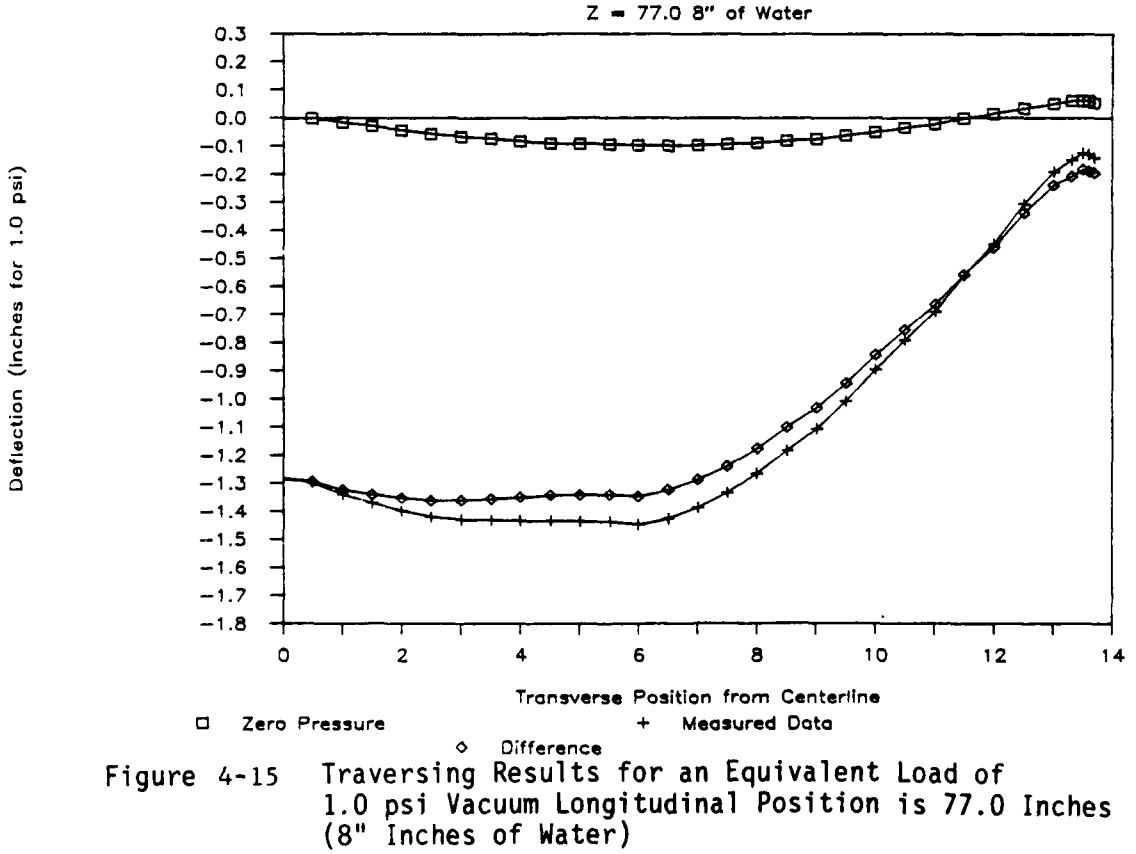

Figure 4-15 Traversing Results for an Equivalent Load of 1.0 psi Vacuum Longitudinal Position is 77.0 Inches (8" Inches of Water)

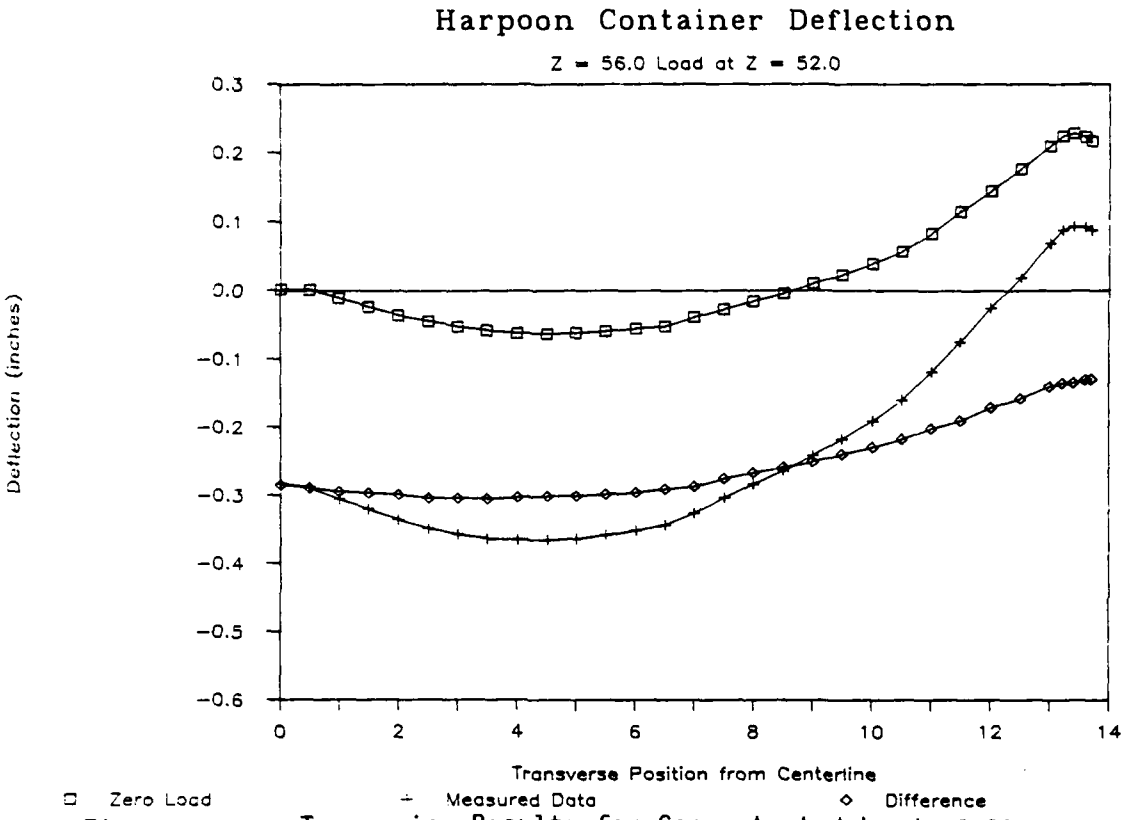

Figure 4-16 Traversing Results for Concentrated Load of 200 lbs Edge Load at Z = 52.0, Displacement at Z = 56.0

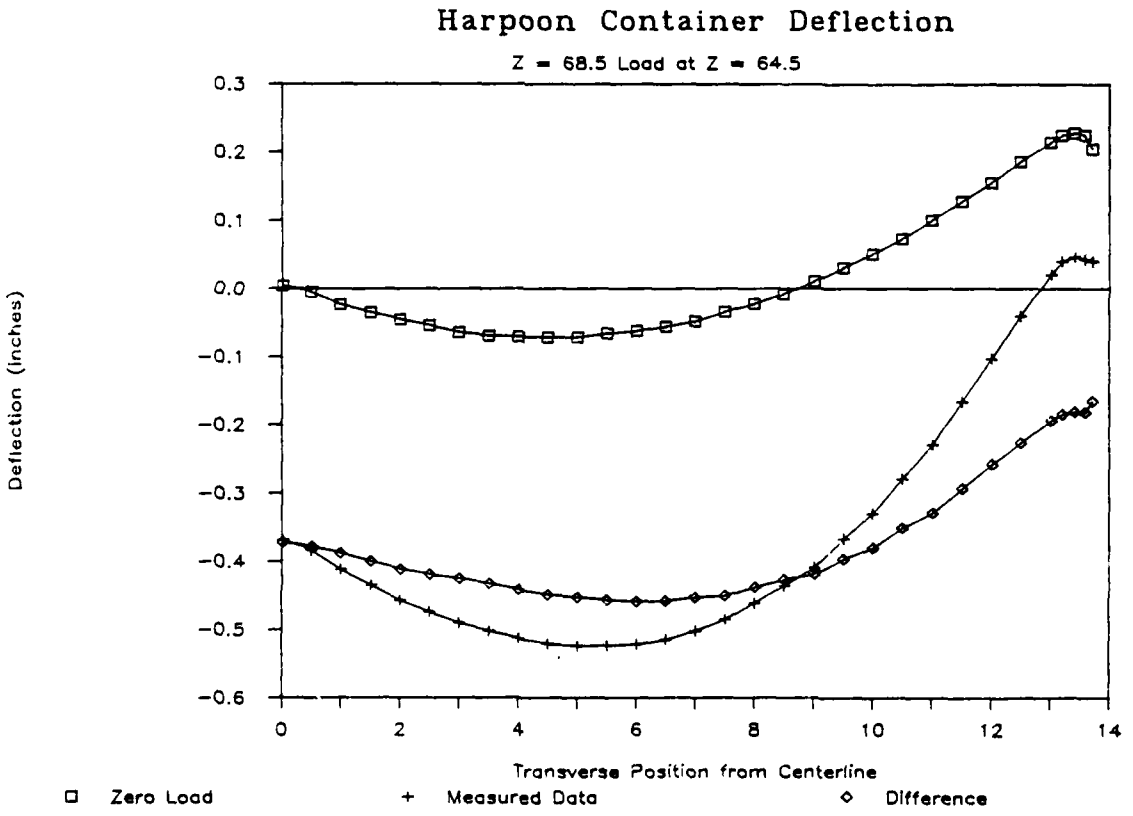

Figure 4-17 Traversing Results for Concentrated Load of 200 lbs Edge Load at Z = 64.5, Displacement at Z = 68.5

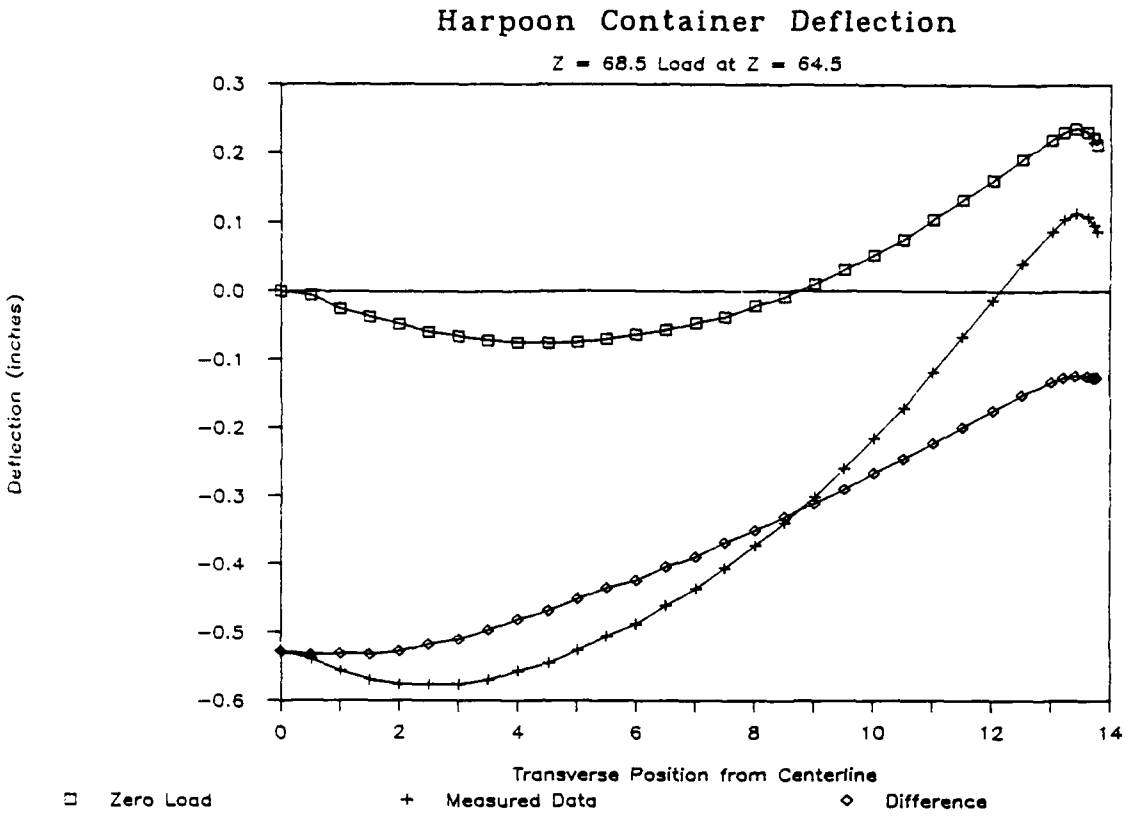

Figure 4-18 Traversing Results for Concentrated Load of 200 lbs Center Load at Z = 64.5, Displacement at Z = 68.5

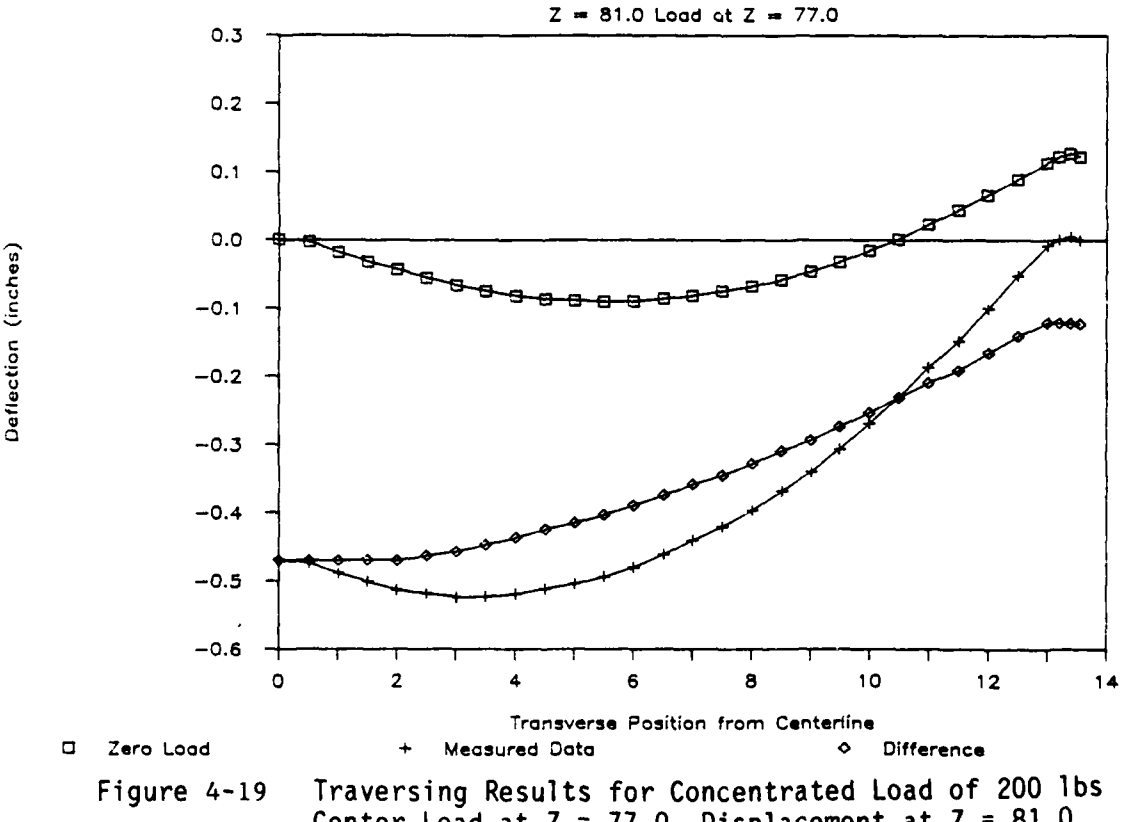

Figure 4-19 Traversing Results for Concentrated Load of 200 lbs Center Load at Z = 77.0, Displacement at Z = 81.0

the transverse centerline. For all locations plotted, the centerline is always lower than the edge of the shell. This condition is most likely the result of creep in the fiberglass as a function of time. This initial geometry will allow for water to collect on the top surface of the shell.

The plots given include three sets of data: two corresponding to each of the measured zero and load conditions and the third corresponding to the difference between the two. This third set corresponds to the amount of deflection due to loading. As with the previous test results, the deflections have been scaled from the applied 14 inches of water (0.5 psi) up to 1.0 psi. For the plots, the horizontal scale corresponds to the transverse position with 0 corresponding to the centerline and 13.6 corresponding to the edge. Displacement values are in inches. These plots present the results of digitizing the original data and replotting to obtain consistent scales.

Deflection under load was as expected. Interpretation of data is based on the calculated deflection due to loading, not the measured deflection. For deflection at the ribs, it is interesting to note that the centerline deflection for the rib at Z = 52.0 (Figures 4-9 and 4-10) is greater than that for the center rib, Z = 77.0 (Figures 4-13 and 4-14). This is the same result obtained in the original set of data. As expected, the deflection of the centerline between the ribs is greater than that at the ribs.

When one examines the rib deflection at the edge, there is a slight increase with increased Z, -0.19 to -0.33 inches for Z = 29.0 to Z = 77.0. The edge deflection is also less between the ribs than at the ribs. In all cases, the edge deflection is downward, which is probably the result of bending in the angled section of the top shell.

The deflections measured on the lip for the data given are summarized in Table 4-1.

Table 4-1. Lip Deflection for Pressure Loading Normalized to 1.0 psi Load

Longitudinal Position (Z in inches)		Lip Deflection (inches)
29.0		-0.089
52.0		-0.077
52.0	Repeat	-0.091
64.5		-0.101
70.75		-0.063
77.0		-0.075
77.0	Repeat	-0.073
77.0	8" of water	-0.083

These values are small and compare favorably with the original data.

A final set of data for the vacuum loading consisted of measuring the deflection at the centerline at Z = 29.0 for several pressures. The results are summarized in Table 4-2.

Table 4-2. Deflection at Centerline for Increasing Vacuum Z = 29.0

Vacuum		Deflection	
Inches of Water	Pressure (psi)	Measured (inches)	Relative to 1.0 psi (inches)
0	0.00	0.00	
4	0.14	0.18	1.29
8	0.29	0.37	1.28
10	0.36	0.46	1.28
12	0.43	0.56	1.30
14	0.51	0.66	1.29

These values at the centerline appear to be very linear.

The overall shape of the deflections is what one would expect under a uniform load with the zero slope at the centerline. One additional measurement was made with an internal vacuum of 8 inches of water. For this, deflected shape normalized to 1.0 psi (Figure 4-15). The deflection in the center portion, 0 to 6 inches, is flatter than that for the 14 inches of water

loading condition. This indicates that, in addition to plate bending and membrane stiffness, there is some geometric stiffness that comes into play.

The concentrated loading results are plotted in Figures 4-16 to 4-19. The first thing to notice is that deflections under this loading are significantly lower than those obtained for the vacuum loading. The first two plots (Figures 4-16 and 4-17) depict to deflections at longitudinal positions Z = 56.0 and Z = 68.5 with the load at the edge of the shell. As would be expected, the deflection for the loading between the rib is greater than loading at the rib. In addition, the rib distributes the load and there is not as much slope in the shell. The second two plots (Figures 4-18 and 4-19) are for longitudinal positions Z = 68.5 and Z = 81.0 with the load at the transverse centerline. For these two cases, the deflections at the edge are similar. The centerline deflection is greater for the load between the rib, but not as great as for the loading cases at the edge. For all concentrated loading conditions, the load is centered at a longitudinal position 4 inches less than the measured displacement position.

During the unloading phase, displacement measurements were made at the transverse centerline. Due to short-term creep, it took approximately five to ten minutes for the deflection to stabilize under each new loading condition. The results are summarized in Table 4-3.

Table 4-3. Concentrated Loading Deflection Results at Transverse Centerline

Load (lb)	Deflection (inches) at Centerline				
	Z = 56.0 Edge	Z = 68.5 Edge	Z = 68.5 Center	Z = 81.0 Center	
0	0.00	0.00	0.00	0.00	
20	-0.04	-0.05	-0.10	-0.05	
40	-0.06	-0.10	-0.20	-0.10	
60	-0.10	-0.12	-0.26	-0.15	
80	-0.12	-0.16	-0.31	-0.20	
100	-0.15	-0.19	-0.36	-0.25	
120	-0.18	-0.23	-0.40	-0.30	
140	-0.21	-0.27	-0.44	-0.35	
160	-0.24	-0.30	-0.47	-0.39	
180	-0.27	-0.34	-0.50	-0.43	
200	-0.28	-0.37	-0.54	-0.47	
200	-0.033	-0.046		-0.031	(lip deflection)

These results indicate that for loads on the edge and the centered load on a rib, the amount of deflection per unit load is fairly consistent. The amount of deflection for the centered load between the ribs is dependent on the level of loading.

5.0 ANALYSIS OF THE HARPOON MISSILE CONTAINER

The structural analyses of the HARPOON missile container described in this report were performed using the Automatic Dynamic Incremental Nonlinear Analysis (ADINA) [2] finite element code. Pre- and post-processing tasks were accomplished with the Graphics-oriented Interactive Finite Element Time-Sharing System (GIFTS) [3] processor package. The computations were performed on a VAX 11/780 computer.

Two separate sets of analyses were conducted: global analyses of the entire container cover and a small-scale local analysis of the stiffener area. The modeling approach and results for each are described below. For the global analyses, computed results are compared to experimentally measured deflections.

5.1 Global Analysis

5.1.1 Model Geometry

Two types of finite elements were used to model the HARPOON container: triangular plate/shell elements and beam elements. The triangular plate/shell elements were used to model all flat surfaces of the container. Beam elements were used to model transverse stiffeners. For the internal pressure load, symmetry of the structure permitted modeling only one quarter of the geometry as shown in Figure 5-1. Concentrated load cases required the entire cover to be modeled. The one-quarter symmetry model contains 402 nodes with 1741 active degrees of freedom, 615 triangular plate/shell elements and 18 beam elements.

The nominal value for shell thickness of 0.185 inches was used for all plate/shell elements. All model dimensions were taken from the drawings for the upper shell of the container [4]. In the global model, cross-sections of the stiffeners were considered to be solid and rectangular. Penetrations existing in the structure were assumed to have no influence on the strength of the areas where damage has been observed. Hence, they were not included in the model.

5.1.2 Material Properties

The upper shell of the container is fabricated from a fiberglass reinforced plastic (FRP), which, for this analysis, is considered to behave as a linear elastic isotropic material. The transverse stiffeners

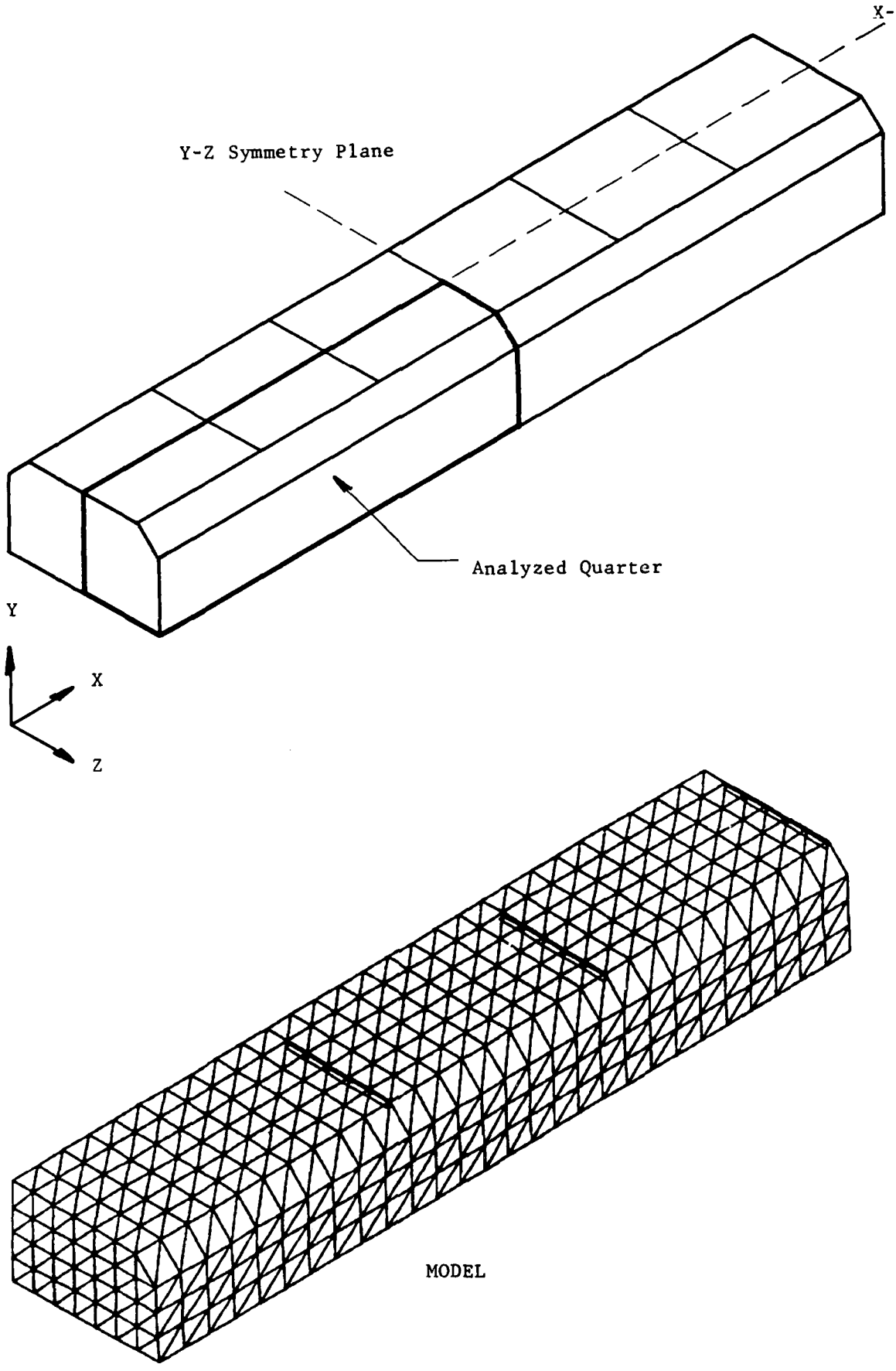

Figure 5-1 Schematic of HARPOON Container Showing Symmetry Planes and Quarter-Symmetry Finite Element Model

are fabricated from expanded polyethylene, coated with fiberglass reinforced plastic.

Material properties used in the finite element model of the upper shell of the HARPOON container were confirmed using experimental measurements from pressure tests. Measured displacements were used to "tune" the material properties of the model such that agreement between experiment and analysis was obtained for a variety of different load conditions.

Values of the Young's modulus for plate/shell elements, E_p, and for beam elements, E_b, were obtained such that the calculated deflections would agree, to engineering accuracy, with the measured experimental data. This adjustment procedure was necessary since available material data was not precise enough for use in an analysis. The values of Young's modulus listed below for the shell and stiffener materials produced deflection results which agreed best with the experiments.

Plate/Shell Material:

$$E_p = 0.97 \times 10^6 \text{ psi}$$

Beam/Stiffener Material:

$$E_b = 0.38 \times 10^6 \text{ psi}$$

The Young's modulus value for the shell material used in the analyses lies within the range of typical values for this material (0.8×10^6 - 1.8×10^6 psi)[5].

5.1.3 Boundary Conditions

The upper shell of the container is attached to the bottom shell in several points and the joint is reinforced with a metal band. The joint is also gasketed to provide a moisture and pressure seal. The degree of restraint provided by this joint was unknown at the outset of the analysis. Two different assumptions were investigated: full rotational restraint and no rotational restraint. The model which permitted rotation at the base of the shell produced deflection results which more closely matched experimental measurements, therefore rotation was permitted at the base of the shell in all subsequent analyses.

5.1.4 Comparison of Global Analysis Results to Experiment

A vacuum was applied to the inside of the container during the experiments to simulate a uniformly applied external load. The numerical analysis was then performed for the case of a uniform external pressure load. Analytical and experimental results are compared for an equivalent

vacuum of 1.0 psi. This value was chosen to permit easy scaling of the results.

Figure 5-2 gives the locations on the container cover at which the calculated results are compared to the measured values. The comparison between analysis and experiment is shown in Figure 5-3 where the measured data are indicated by the isolated symbols in the figure. Comparisons are along the centerline, the quarter-point line (midway between the center and the edge), and along the edge of the container. The analysis predicts deflections quite well in the interior of the shell, however, the model is quite stiffer at the edge of the shell. Based on this agreement, the material properties of the analytical model were judged to satisfactorily represent the actual FRP behavior.

Analyses performed under an internal pressure of +1.0 psi produced shell deflections almost identical to those shown in Figure 5-3 but in the opposite direction. The two-way pressure relief valve mounted on the container cracks to permit flow at an actual internal (or external) pressure differential of 0.5 psi, +/- 0.25 psi [6]. Since linear elastic behavior is assumed, actual deflections can be obtained by scaling the deflections in Figure 5-3 by the pressure magnitude in the appropriate direction.

To simulate "footprint loads", concentrated loads of 200 lbs were separately applied to the container top surface at the four different locations shown in Figure 5-4. Vertical deflections were measured at the locations described previously. Three of the load cases were nonsymmetric and required the development of a larger finite element model of the entire upper shell structure. This larger model contains 1439 nodes having 6877 active degrees of freedom; 2380 plate/shell elements and 60 beam elements were used. Figures 5-5 through 5-8 compare measured vertical deflections with calculated vertical deflections for each concentrated load case. Reasonable agreement is demonstrated; the best comparison occurs for load cases number 1 and 3. As expected, the maximum deflection (0.9 inches) is calculated for load case 2 with the concentrated load located at the center of a panel between the stiffeners. For each concentrated load case, the resulting stresses were much lower than those calculated for the internal pressure loading.

The above comparisons demonstrate the accuracy of the finite element model of the upper shell container. Stresses calculated in the above

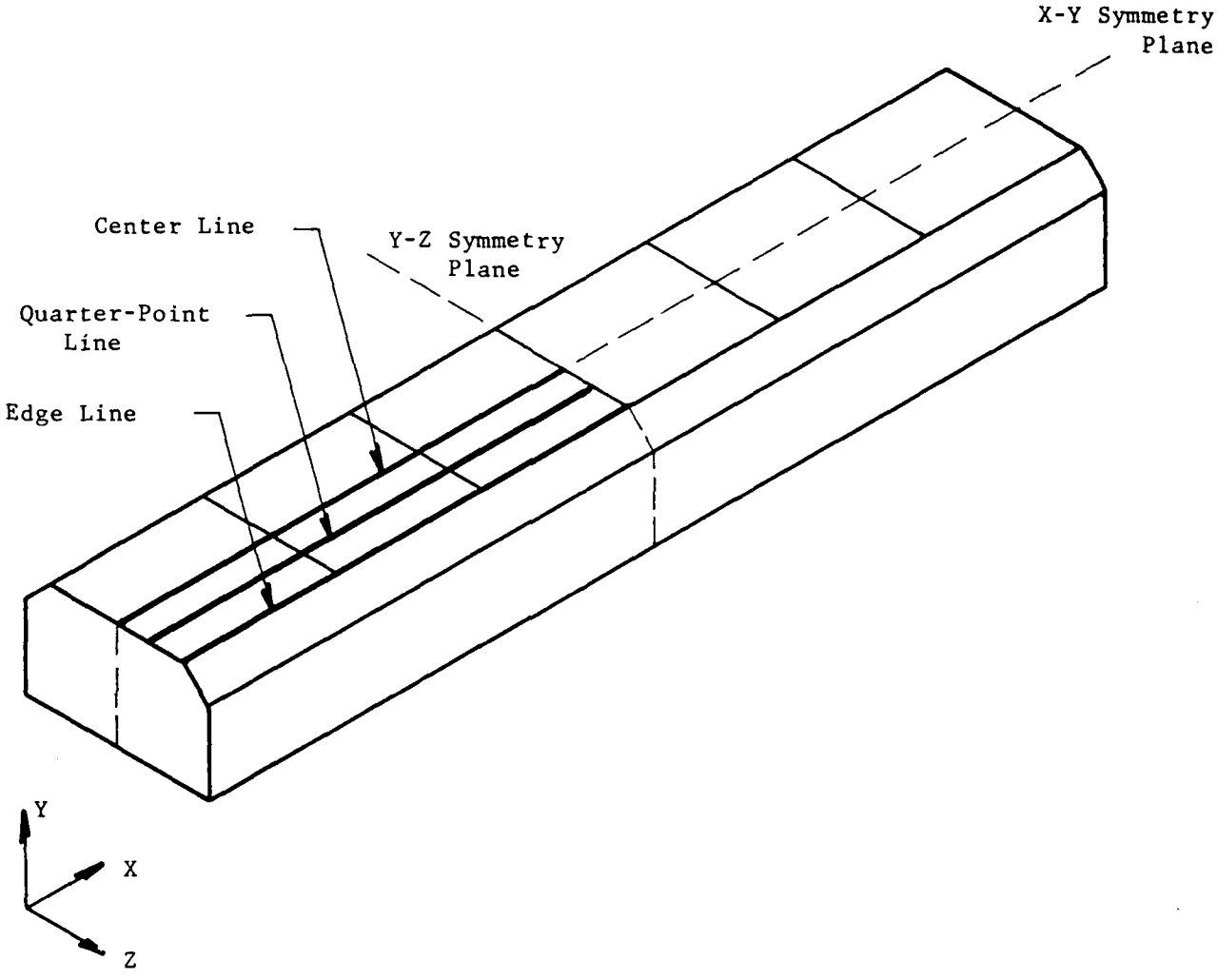

Figure 5-2 Longitudinal Lines for Comparison of
Calculated and Measured Deflections

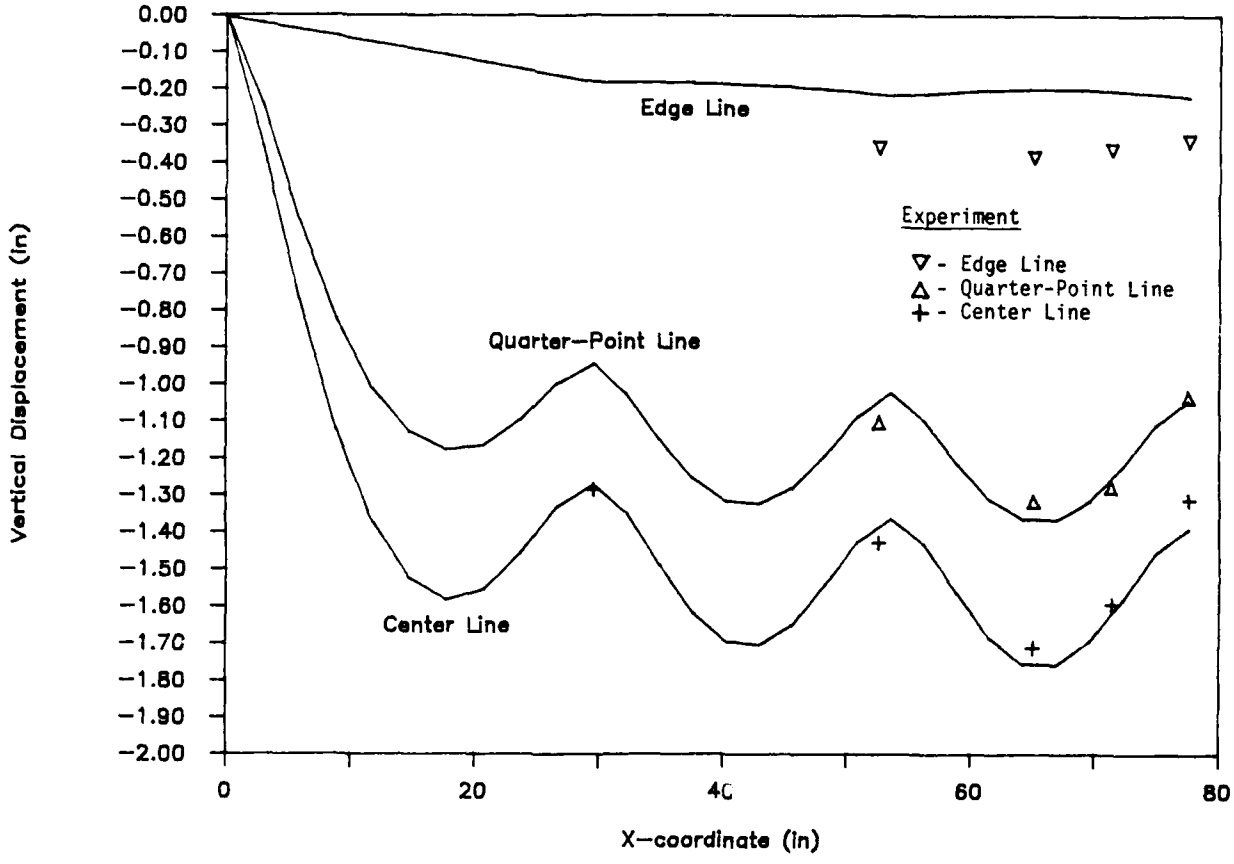

Figure 5-3 Comparison of Calculated and Measured Vertical Deflections for an Internal Vacuum of 1.0 psi

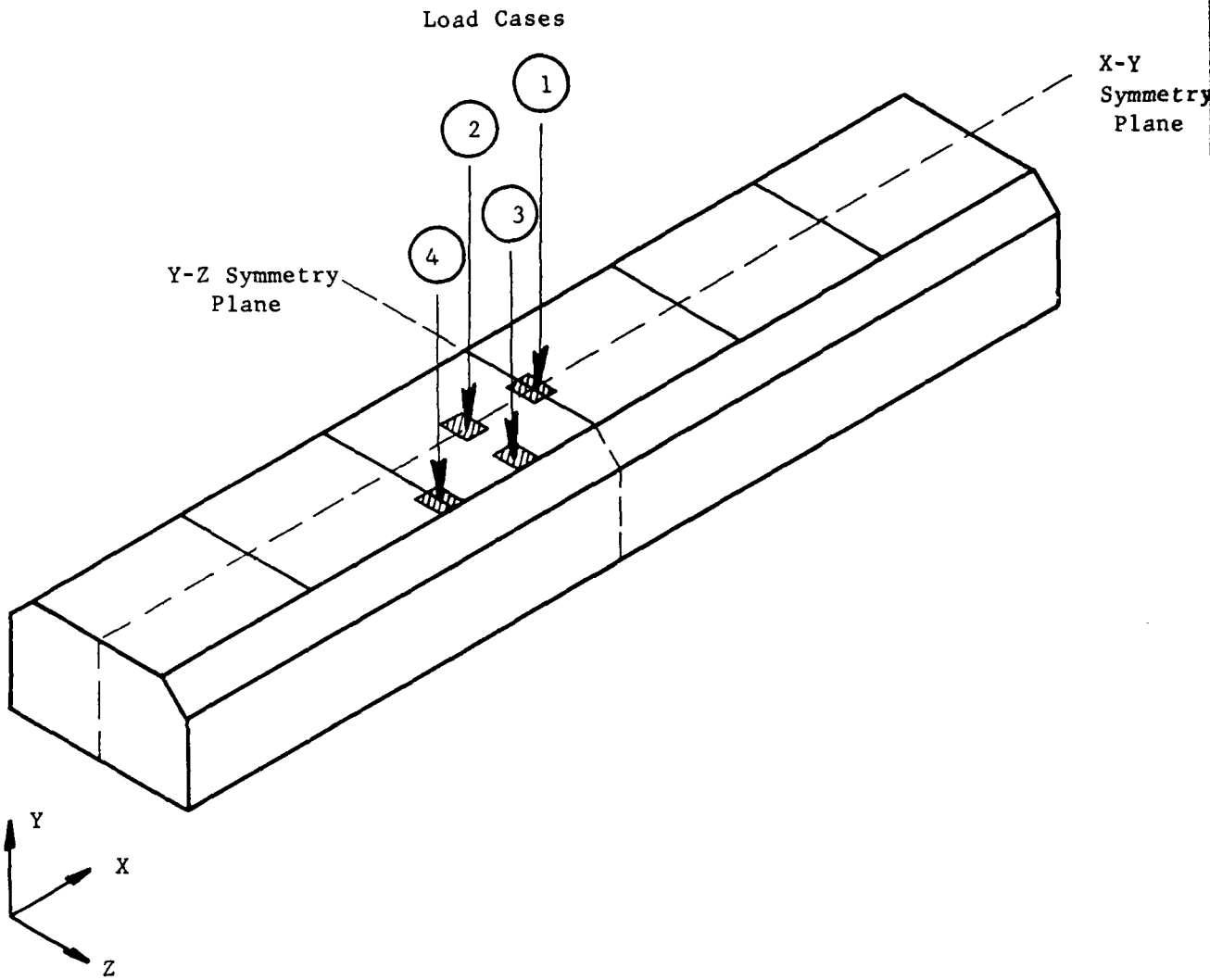

Figure 5-4 Location of 200 lb Concentrated Loads

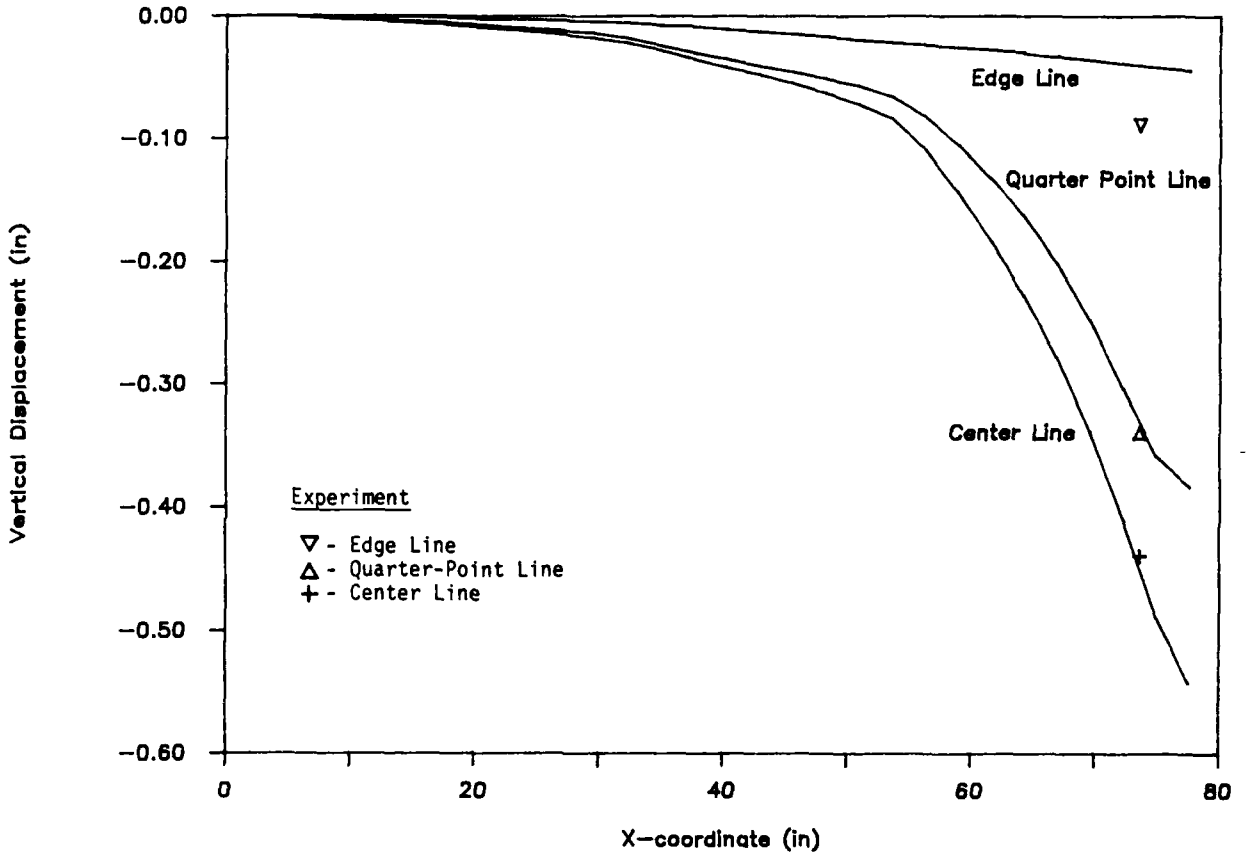

Figure 5-5 Comparison of Calculated and Measured Vertical Deflections for Concentrated Load Case Number 1

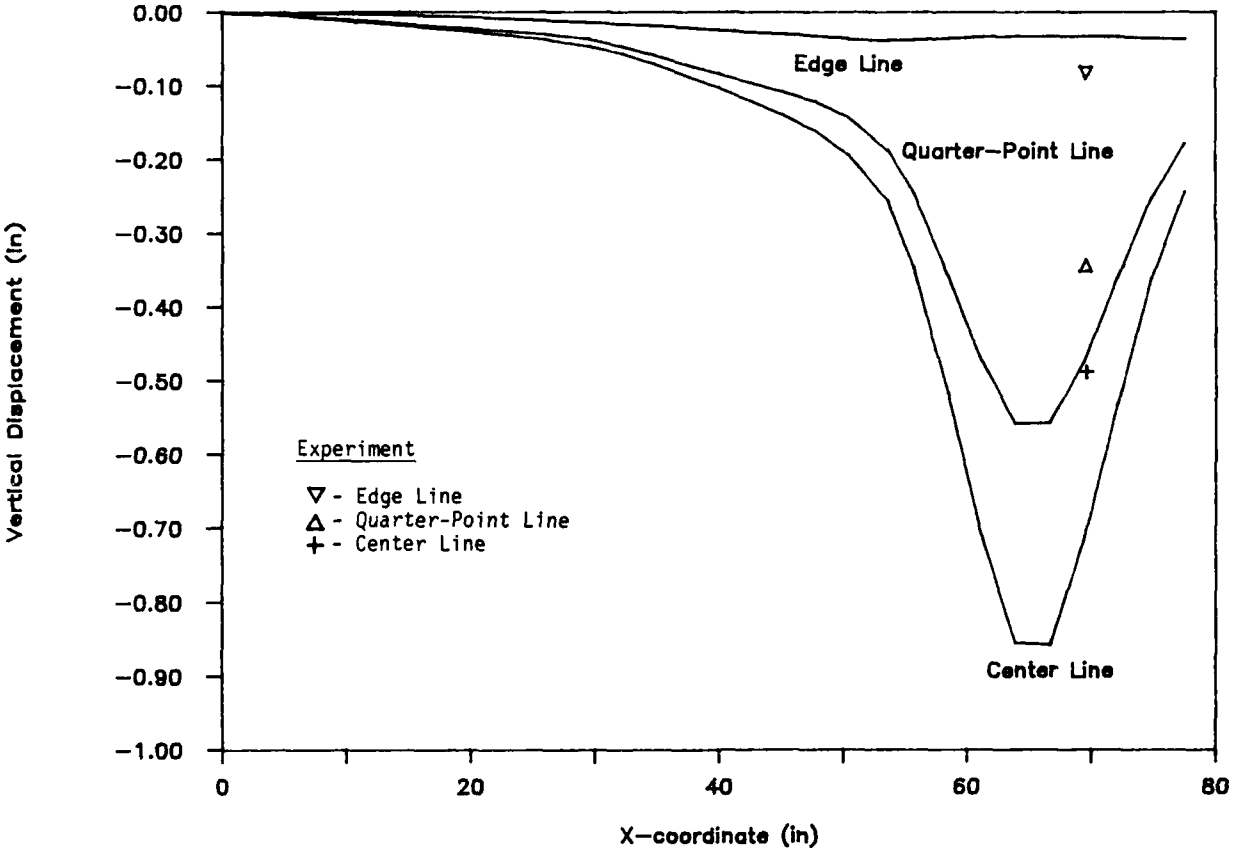

Figure 5-6 Comparison of Calculated and Experimentally Measured Vertical Deflections for Concentrated Load Case Number 2

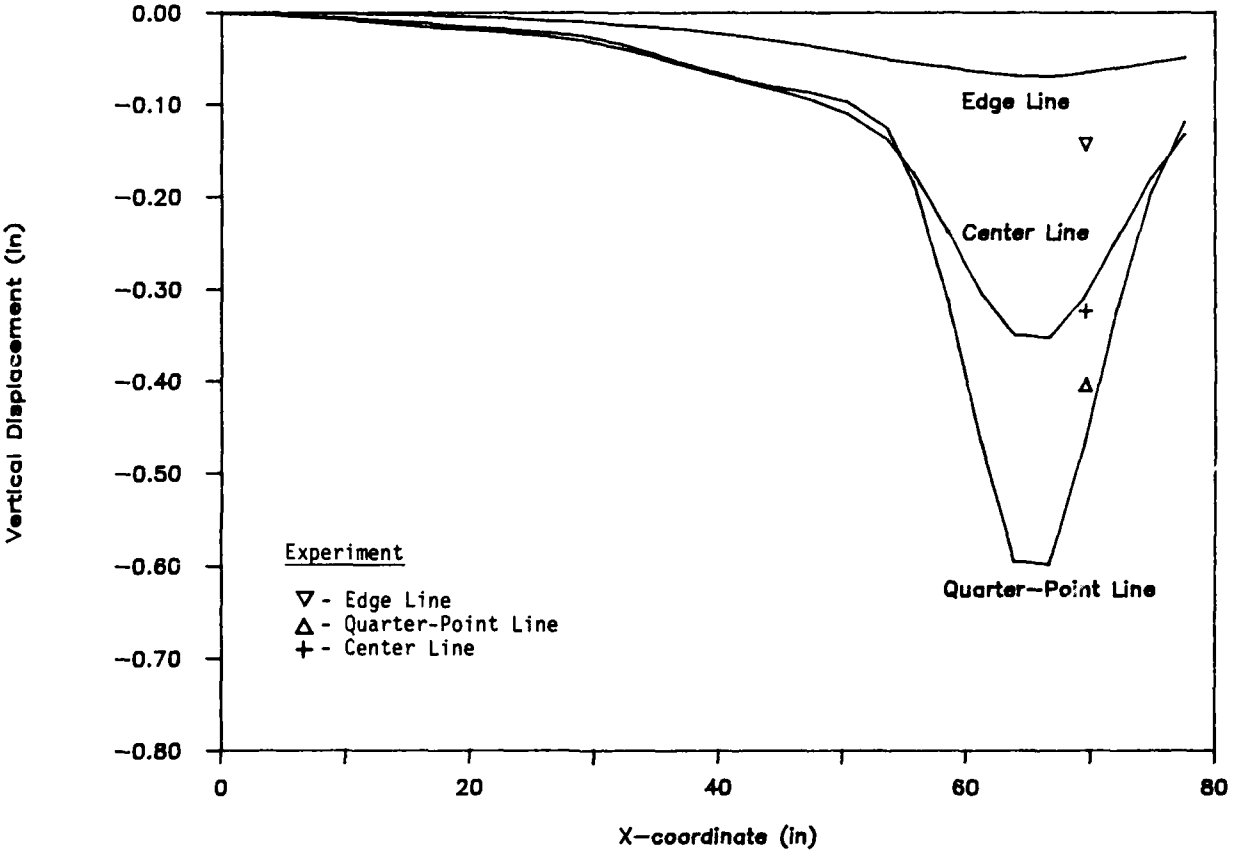

Figure 5-7 Comparison of Calculated and Experimentally Measured Vertical Deflections for Concentrated Load Case Number 3

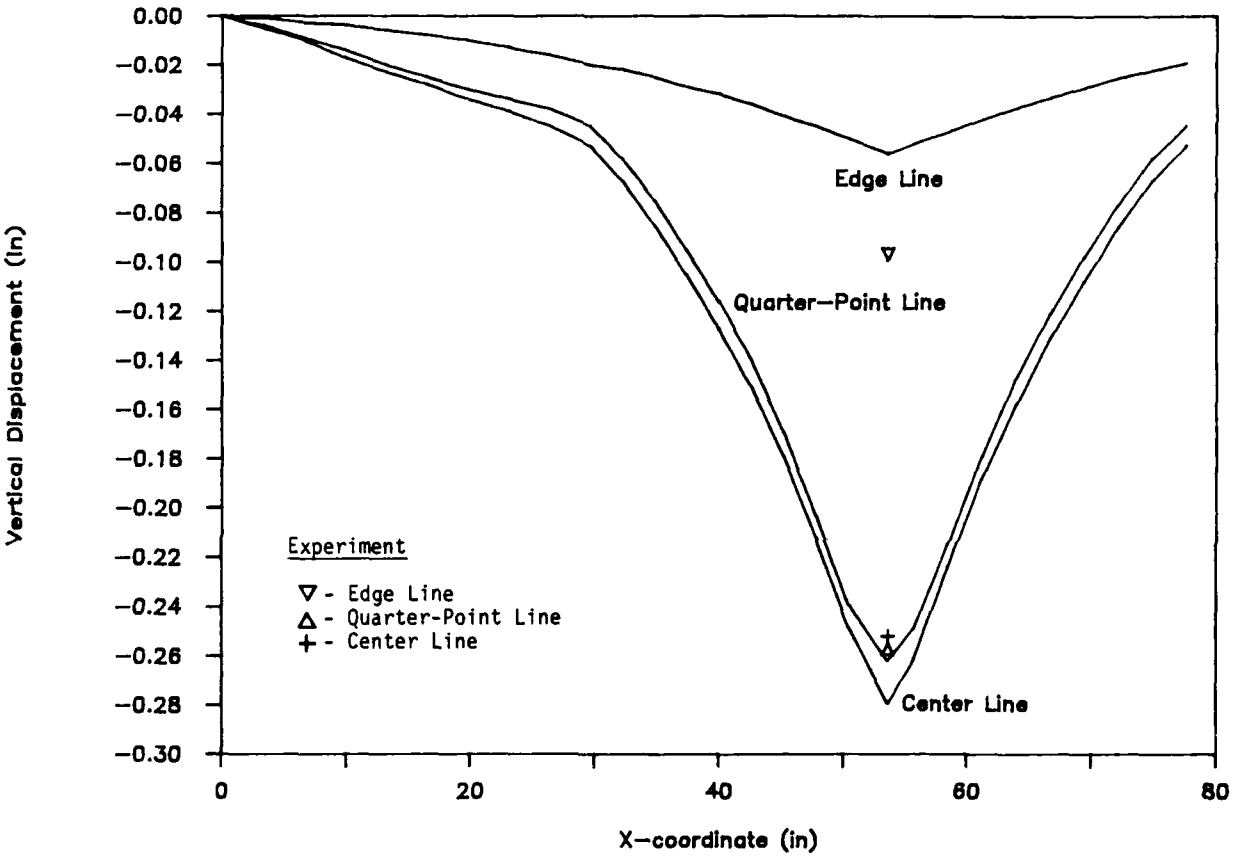

Figure 5-8 Comparison of Calculated and Experimentally Measured Vertical Deflections for Concentrated Load Case Number 4

analyses were low (less than 1,200 psi), well below yield stresses typically quoted for this material (S_{ymin} = 9,000 psi)[5]. Therefore, it is inconceivable, based on the stress results from the above analyses, to see how the above uniform pressure loadings could have caused the observed panel cracking (failure mode I). However, a potential cause for the mode I failures has been identified using the calculated deflections. This scenario is discussed in Section 6.0.

5.2 Local Analysis of Stiffener

The global analyses described above used a simplified beam element geometry to model the stiffeners and did not permit a precise evaluation of the stresses in and near the stiffeners. For this reason, a more detailed "local" analysis of a container stiffener was performed by applying deflections calculated from the global analysis to a detailed stiffener model. It was also hoped that this local analysis would provide insight into the mode II failures.

5.2.1 Model Geometry

The area of the container selected for modeling in the local analysis is shown in Figure 5-9 along with a three-dimensional view of the model. Triangular plate/shell finite elements were used in the local analysis model of the stiffener. The entire model contained 834 elements and 427 nodes having 2562 degrees of freedom. The detailed model of the stiffener is comprised of an effective flange width of the container shell and an open section approximating the actual shape of the stiffener. The effective flange width of 4.0 inches was determined using the standard engineering practice that applies to symmetric T-beams [7].

5.2.2 Material Properties

The outside portion of the stiffener is fabricated with a composite of 30% woven glass cloth (3 layers) and 70% resin [4], a composition considered similar to that of the shell material. Hence, the elastic modulus and Poisson's ratio of the shell material was also employed to model the outside portion of the stiffener. For this detailed model of the stiffener, the expanded polyethylene (ethafoam) stiffener interior is considered to be non-loadbearing. The assumption that the polyethelyene carrys no load is based on the supposition that it acts primarily as a "spacer" to provide shape to the woven glass cloth and resin before it cures.

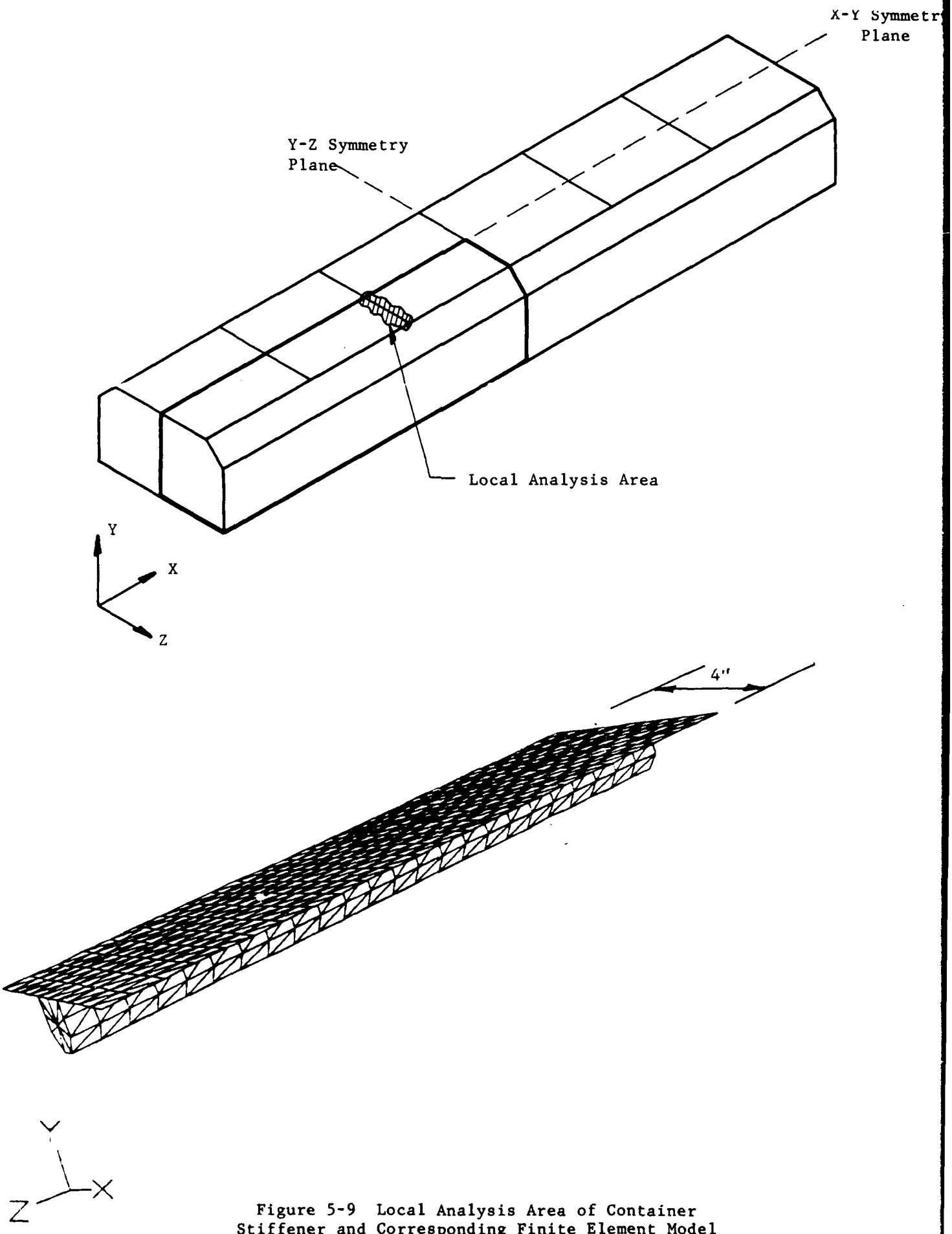

Figure 5-9 Local Analysis Area of Container Stiffener and Corresponding Finite Element Model

To insure that bending behavior of the local stiffener model matched that of the global container model, the bending stiffness (EI) of the local model was equated to that of the global model. Thus, the thickness of the stiffener section was calculated to be 0.07 inches. A cross-section of the model of the stiffener is given in Figure 5-10, along with the corresponding drawing from Reference [4]. Note that the drawing calls out a thickness of 0.38 inches; however, the individual glass cloth layer thickness is not specified. Also, there is a large tolerance (+/-10%) on the chamfer. Recognizing that these stiffeners are laid-up by hand raises concern over the accuracy of the as-built thickness. Given the above ambiquities, it was decided to preserve the deflection behavior of the stiffener by using a thickness of 0.07 inches in the local model and employ material properties of the shell.

If specific material data were available for the stiffener lay-up, the thickness specified in Reference 4 could have been used in the local model. The modeling approach described above was followed as a means to obtain a reasonable engineering estimate of what bending stresses may exist in the stiffeners of the HARPOON container.

5.2.3 Local Analysis Results

Deflections calculated by the global analysis of the HARPOON container under internal pressure load were applied to the local model of the stiffener. For a pressure differential of 0.75 psi, the maximum permitted by the two-way pressure relief valve, von Mises equivalent stresses were calculated to be on the order of 9900 psi near midspan of the stiffener.

These maximum stress levels calculated at the midspan of the stiffener agree with the locations where cracks have indeed occurred; see Figure 2-1. This result is entirely reasonable and expected, since the maximum bending moment would occur at midspan. Yield strengths for the FRP material are quoted to be in the range of 9-18 ksi [5]. Given the variability in this material property, the modeling approximations used, and assuming that the yield stress of the hand laid-up stiffener is approximately equal to that of the FRP, it can be concluded that the stress state near the stiffener midspan may be on the threshold of causing failure. A precise definition of both the geometry and the material of the stiffener would enable a more conclusive analysis to be performed. At present, however, a definite statement concerning the origin of the mode II failures cannot be made.

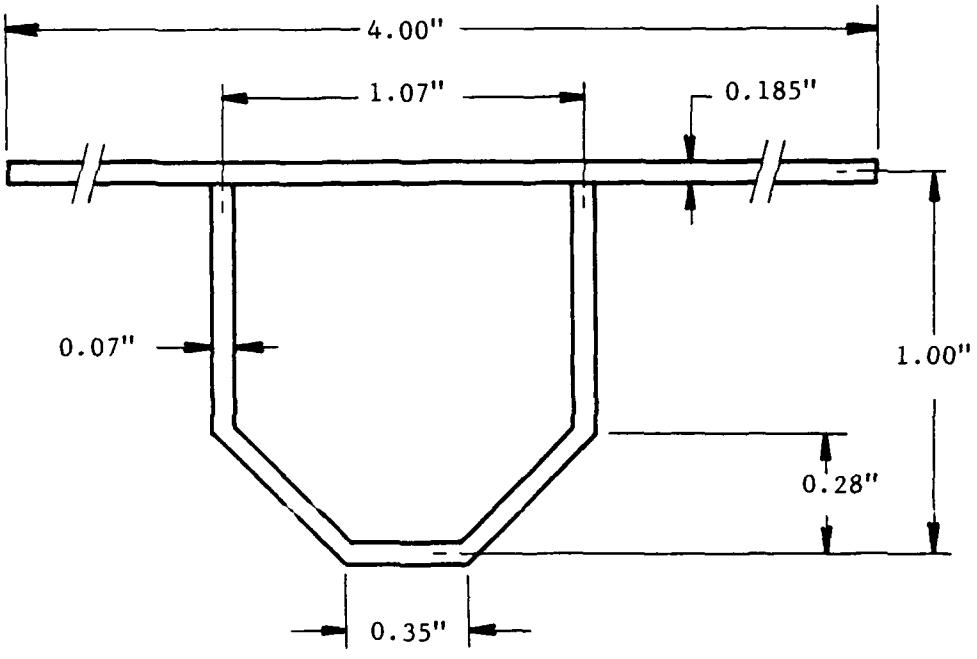

a. Cross-section of Stiffener Used in Local Finite Element Model

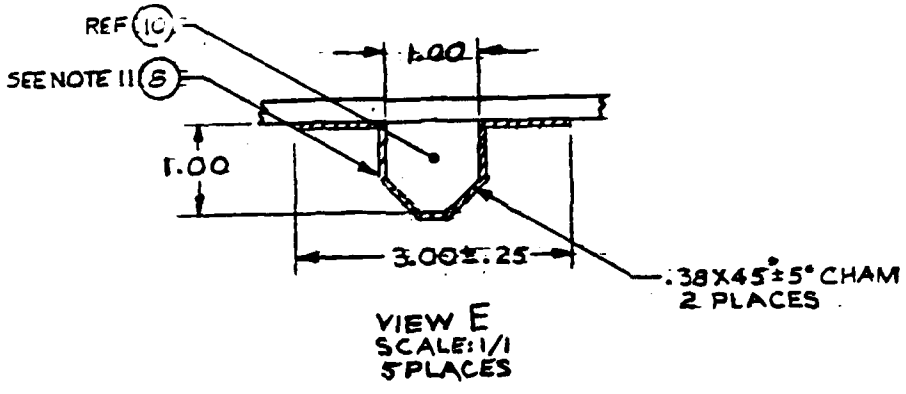

b. Cross-section of Stiffener as Specified by Reference [4]

Figure 5-10 Cross-sections of Container Stiffener

6.0 DISCUSSION OF ANALYTICAL RESULTS RELATIVE TO OBSERVED DAMAGE

The global structural analyses performed on the HARPOON container provided no indications as to why the panel cracking (failure mode I) was occuring. Stresses in the panels were calculated to be well below yield (9,000 psi) for all loading cases considered. Thus, the cause of the panel cracking was unexplained by the analytical study. Therefore, SwRI sought other scenarios which could cause the observed damage.

The most likely scenario which could produce the cracking observed in the panels can be developed by examining Figures 2-1, 2-2, and 6-1. Figure 2-1 shows the underside of the damaged cover illustrating the locations of the damage on the panels. An enlargement of this damage is shown in Figure 2-3. The two damaged areas are estimated to be about 3.5 inches apart and have an approximate diameter of 0.5 inches. Figure 6-1 gives an uncovered view of a HARPOON container, with the missiles removed, showing the interior missile support saddles. Observe that, in the center of the container, the threaded ends of pairs of bolts protrude upward from the missile support saddles. Noting that these saddles are near the center of the container, that the damage occurs near the center of the container (Figure 2-1), and that the damage occurs in paired locations (Figure 2-3), we postulate that the damage is a result of the upper shell of the container coming into contact with the ends of the bolts on the missile support saddles. A review of the container drawings [4,8,9] indicates that, in the undeformed state, the clearance between the inside surface of the cover and the top of the bolts is a **maximum** of 0.5 inches.

Using the deflection results of the previous analyses, and the principle of superposition, an expression can be developed to calculate the clearance, or gap, remaining between the panel and the top of the bolts when loads are applied to the container. The remaining gap, G, is a function of the initial gap, G_o, a postulated external concentrated load, F, acting at the center of the panel, and the differential pressure, Δp, equal to the difference between the interior and the exterior pressures:

$$G = G_o + 0.0045F + 1.75\ \Delta p$$

In this equation, G and G_o are assumed to be in inches, F in pounds, and Δp in psi. To illustrate the use of the expression, consider the case

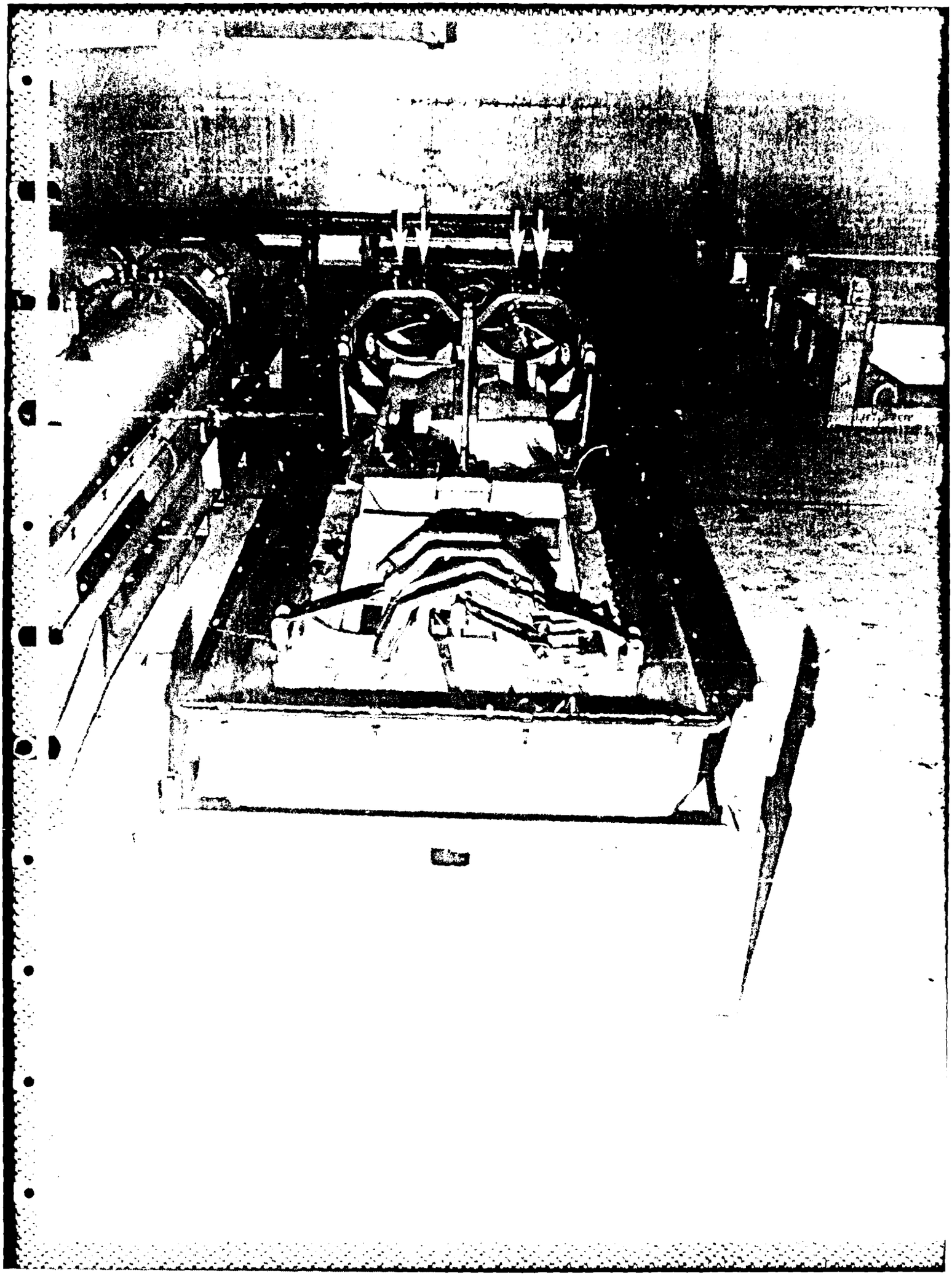

where the differential pressure is zero and a 200-lb concentrated force acts at the center of the panel. The sign of the force F should be consistent with the coordinate system shown in Figure 5-4; i.e., F acts in the negative y-direction. Taking the initial gap, G_o, to be equal to 0.5 inches, the equation gives:

$$G = 0.5 + 0.0045(-200) + 1.75(0) = -0.4 \text{ in.}$$

Since the result is negative, contact between the bolt and the panel will occur under this load.

A second case that may be considered is that of an internal vacuum (negative Δp) or an externally applied pressure load acting alone. For example, if the pressure relief valve stuck at a Δp of -0.4 psi then the equation gives:

$$G = 0.5 + 0.0045(0) + 1.75(-0.4) = -0.2 \text{ in.}$$

Again, contact is predicted. Obviously, a combination of each of these two load cases could also induce contact.

Under the conditions postulated above, the shell cover can come into contact with the bolts on the top of the missile saddles. These simple calculations were not intended to be rigorous in nature. Rather, they were performed to demonstrate, using a range of realistic parameters, that contact between the container cover and the interior missile saddle could indeed occur, resulting in damage to the cover.

The above reasoning is also supported by the actual spacing of the bolts (3.5 inches on center) and their diameter (0.625 inches) as given by the container drawings [9,10]; see Figure 6-2. These figures are similar to the dimensions used to size the damage in Figure 2-3. Therefore, we conclude, on the basis of the observed damage locations and pattern, the results of the structural analysis calculations, and the configuration of the missile support saddle bolts, that **the cracking observed on the exterior of the container was caused by the cover being deflected downward onto the missile saddle bolts.**

The specific cause of the deflection that results in the contact between the bolts and the cover remains unknown. However, the cases postulated above for the sample calculations are likely load scenarios which could induce the damage corresponding to failure mode I. A likely cause was not identified for failure mode II.

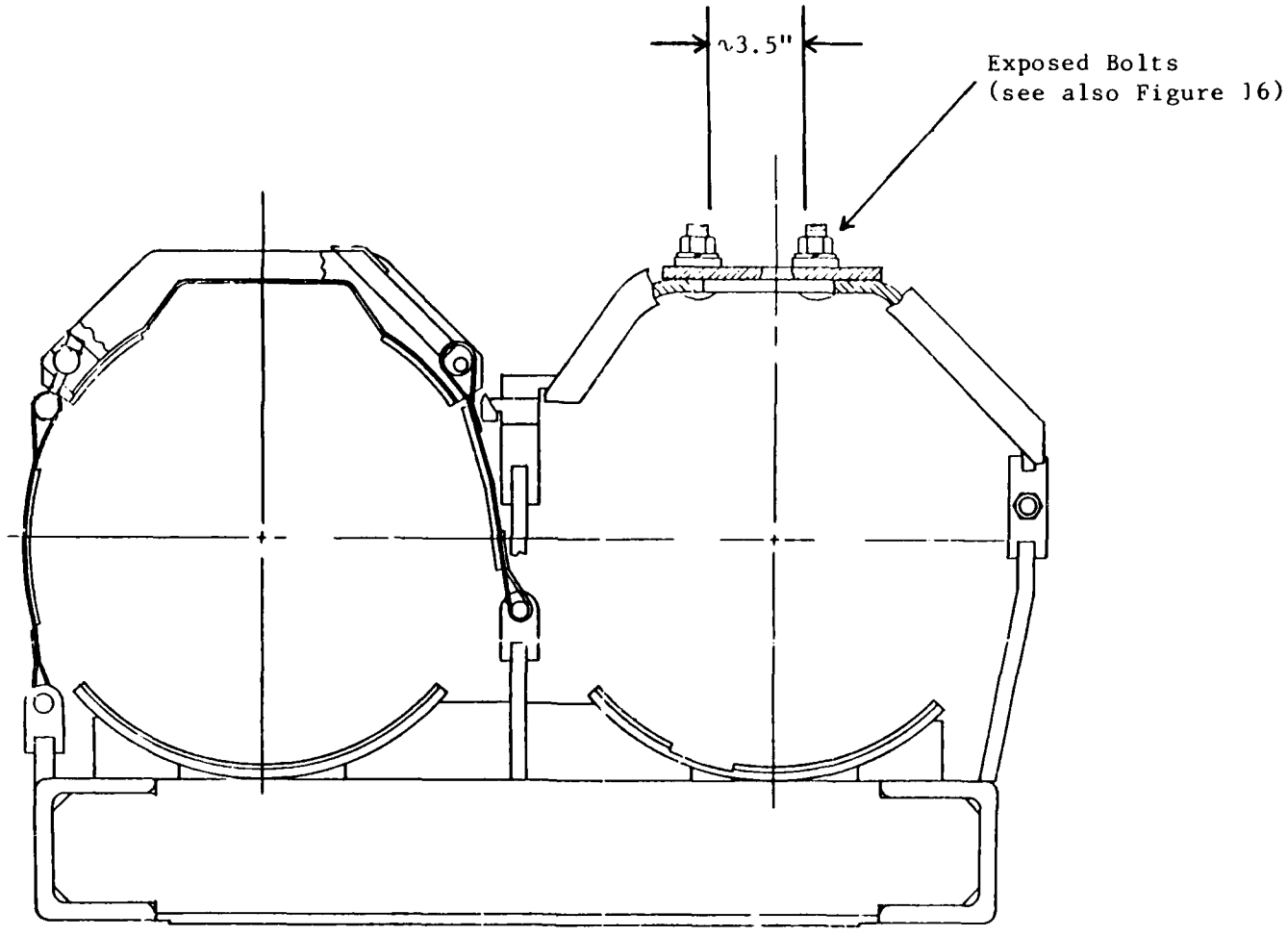

Figure 6-2 Drawing of Missile Support Saddle Showing Location and Size of Protruding Bolt Shafts (from Reference [9])

7.0 RECOMMENDATIONS

The most straightforward method of eliminating the cracking of the container (failure mode I) cover would be to implement operational procedures which preclude the HARPOON containers from being loaded from the exterior. Walking or sitting on the container should not be permitted, nor should heavy objects be allowed to rest on the container. This recommendatiom could be implemented by painting a "NO STEP" warning on the upper surface of the container cover.

In addition, the design of the missile saddle could be modified such that the ends of the bolts are oriented away from the cover (i.e., turned inward; see Figure 6-2), or a shield over the ends of the bolts should be installed to prevent contact with the cover, or both. If neither of these latter alternatives are practical, an alternate design of the saddle should be developed such that, if the saddle comes in contact with the cover, damage to the cover is precluded.

Because of the uncertainties discussed in Section 5.2. it is difficult to offer a specific recommendation to remedy the mode II failures. Therefore, it is recommended that the geometry and material properties of the stiffener be defined more precisely to facilitate a more accurate analysis of the mode II failures.

Further investigations, both experimental and analytical, would be beneficial in resolving the HARPOON container failures. The scenario postulated for the contact between the container cover and the bolts of the missile support bracket could be studied using a container and either the actual or a mock-up of the missile support brackets. Exterior loads could be applied to the container to identify at what load level contact actually occurs.

It has also been speculated that vibration of the container cover may contribute to the observed damage. Dynamic testing and analyses to identify critical vibration frequencies would determine whether or not the dynamic response of the container is a contributing factor to the observed damage.

Finally, a forensic examination (failure analysis) of actual container mode I and II damage would be valuable in identifying the cause of the failures.

8.0 REFERENCES

1. NAVAIR 11-75CNT-1, General Fiberglass Repair Procedure for HARPOON Container, February 1984.

2. "ADINA User's Manual," Report AE 81-1, ADINA Engineering, Inc., September 1981.

3. "GIFTS User's Manual," Version 5.03, University of Arizona, April, 1981.

4. HARPOON Missile Container, MK 607, Drawing No. F-10001-2645444.

5. "FRP - An Introduction to Fiberglas-Reinforced Plastics," Owens-Corning Fiberglas Corporation, Toledo, Ohio, 1976.

6. HARPOON Missile Container, MK 607, Drawing No. C-10001-2645538.

7. Wang, C-K., and Salmon, C.G., Reinforced Concrete Design, Intext, New York, 1973, p. 281.

8. HARPOON Missile Container, MK 607, Drawing No. F-10001-2645309.

9. HARPOON Missile Container, MK 607, Drawing No. F-10001-2645428.

10. HARPOON Missile Container, MK 607, Drawing No. C-10001-2645435.

END

DATED

FILM

9-88

DTIC